

ISSN 0036-8075
12 JULY 1996
VOLUME 273
NUMBER 5272

SCIENCE



AMERICAN
ASSOCIATION FOR THE
ADVANCEMENT OF
SCIENCE

NEWS

The Decline of German Universities	172
Foreign Students Bypassing Germany	173
Disputed Results Now Just a Footnote	174
Panel Backs Joint Bion Mission	175
Earmark for New Ship Puts Academics Over Pork Barrel	176
Italian Bioethics: Embryo Report Opens Old Wounds	177
Publisher Draws Censorship Charge	177
Tobacco Studies: UC Objects to Research Restrictions	178
Silver Thread Boosts Current Capacity	178
Unruly Sun Emerges in Solar Observatory's First Results	179
Spying On the Sun—on the Cheap	180
Evolutionary and Systematic Biologists Converge	181
Twinkle, Twinkle, Little Quasar	182

Protein Matchmaker May Lead New Gene Therapy to the Altar	183
---	-----

SPECIAL NEWS REPORT

Putting Prions to the Test	184
Flipping Yeast	186
Prusiner and the Press	188

PERSPECTIVES

If a Tree Falls in the Forest...	201
M. Keller, D. A. Clark, D. B. Clark, A. M. Weitz, E. Veldkamp	

The Shrewd Grasp of RNA Polymerase	202
R. Landick and J. W. Roberts	

Rho Returns: Its Targets in Focal Adhesions	203
H. Bussey	

ARTICLE

New Designs of Macroporous Polymers and Supports: From Separation to Biocatalysis	205
F. Svec and J. M. J. Fréchet	

184

Do prions mangle proteins?

DEPARTMENTS

THIS WEEK IN SCIENCE	157	RANDOM SAMPLES	191
EDITORIAL	163	High Court Won't Review <i>Hopwood</i> • Manatee Killer Revealed • Canada Considers Gene Law	
Scientific Imagination and Integrity			
K. J. Ryan		BOOK REVIEWS	196
LETTERS	165	<i>Bendectin and Birth Defects</i> , reviewed by S. Bartlett Foote • <i>The Mismeasure of Man</i> • <i>The World According to Wavelets</i> • <i>Wavelets</i> • Vignette • Books Received	
Not the "Dark Ages": W. C. Barker and R. S. Ledley • Dinosaurs and Their Youth: M. A. Norell and J. M. Clark; N. R. Geist and T. D. Jones • Tobacco Research: J. F. Glenn; J. Cohen; T. D. Sterling • Uninterrupted Electric Power: D. N. Baker and J. G. Kappenman		PRODUCTS & MATERIALS	262
SCIENCESCOPE	171	SCIENCE'S NEXT WAVE	265
		Bioinformatics: New Frontier Calls Young Scientists	

AAAS Board of Directors

Rita R. Colwell
Retiring President, Chairman
Jane Lubchenco
President
Mildred S. Dresselhaus
President-elect

Sheila Jasanoff
William A. Lester Jr.
Simon A. Levin
Marcia C. Linn
Michael J. Novacek
Anna C. Roosevelt
Jean E. Taylor
Nancy S. Wexler

William T. Golden
Treasurer
Richard S. Nicholson
Executive Officer

■ SCIENCE (ISSN 0036-8075) is published weekly on Friday, except the last week in December, by the American Association for the Advancement of Science, 1200 New York Avenue, NW, Washington, DC 20005. Periodicals Mail postage (publication No. 484460) paid at Washington, DC, and additional mailing offices. Copyright © 1996 by the American Association for the Advancement of Science. The title SCIENCE is a registered trademark of the AAAS. Domestic individual membership and subscription (51 issues): \$102 (\$55 allocated to subscription). Domestic institutional subscription (51 issues): \$250. Foreign postage extra: Mexico, Caribbean (surface mail) \$55; other countries (air assist delivery) \$90. First class, airmail, student, and emeritus rates on request. Canadian rates with GST available upon request, GST #1254 88122. Printed in the U.S.A.

Structure of the FKBP12-Rapamycin Complex Interacting with the Binding Domain of Human FRAP

Jungwon Choi,* Jie Chen, Stuart L. Schreiber, Jon Clardy†

Rapamycin, a potent immunosuppressive agent, binds two proteins: the FK506-binding protein (FKBP12) and the FKBP-rapamycin-associated protein (FRAP). A crystal structure of the ternary complex of human FKBP12, rapamycin, and the FKBP12-rapamycin-binding (FRB) domain of human FRAP at a resolution of 2.7 angstroms revealed the two proteins bound together as a result of the ability of rapamycin to occupy two different hydrophobic binding pockets simultaneously. The structure shows extensive interactions between rapamycin and both proteins, but fewer interactions between the proteins. The structure of the FRB domain of FRAP clarifies both rapamycin-independent and -dependent effects observed for mutants of FRAP and its homologs in the family of proteins related to the ataxia-telangiectasia mutant gene product, and it illustrates how a small cell-permeable molecule can mediate protein dimerization.

A dividing cell must pass various checkpoints as it proceeds through the cell cycle, and error-free division requires the ability to rectify DNA lesions (1, 2). The ataxia-telangiectasia mutant (ATM) gene product, the catalytic subunit of the DNA-dependent protein kinase, and the products of yeast genes such as *TOR1*, *TOR2*, and *MEC1* (*ESR1*) are members of a family of large molecular size proteins that participate in cell cycle progression and checkpoints as well as in DNA repair and recombination (1–4). All members of the ATM family contain a COOH-terminal kinase domain (1–4), but no structural information is available for any domain of any family member. Human FRAP (rat RAFT), one member of this family, is a 289-kD protein that binds FKBP12-rapamycin, regulates p70 ribosomal protein S6 kinase, and is required for G_1 cell cycle progression in several cell types (5–7).

The potent immunosuppressive agents FK506 (8) and rapamycin (9–11) (Fig. 1A) share the same cellular target: the 12-kD FK506-binding protein, FKBP12 (12, 13). Although both rapamycin and FK506 bind to FKBP12 with high affinity [dissociation constant (K_d), 0.2 to 0.4 nM], they effect immunosuppression through different mechanisms. Whereas FK506 interrupts the signal from the T cell receptor, rapamycin interrupts the signal from the interleukin-2 receptor and the receptors for other cytokines and growth factors (14). Binding of similar molecules, such as FK506 and rapamycin,

to the same protein can disrupt different signals because the protein-ligand complexes, (not the individual components) are the active entities (14). FKBP12-FK506 inhibits calcineurin, a serine-threonine phosphatase (15), whereas FKBP12-rapamycin binds to FRAP (5). Thus, small cell-permeable molecules can induce proteins to associate in a manner similar to that by which growth factors (such as human growth hormone), cytokines (such as interleukin-2), and intracellular signaling proteins (such as GRB2) induce dimerization of signaling proteins. These naturally occurring inducers of dimerization have inspired the design of synthetic molecules that induce dimerization of intracellular proteins and result in the activation of cytoplasmic signaling pathways (16).

FK506 and rapamycin bind FKBP12 in a hydrophobic pocket, and an important feature of both FKBP12-ligand structures is the large fraction, ~50%, of ligand exposed on the exterior of the complex (17–19). A composite surface—a surface with contributions from both ligand (FK506 or rapamycin) and the protein (FKBP12)—mediates the interaction of the FKBP12-ligand complex with its target (14). Two independent x-ray structures of the ternary FKBP12-FK506-calcineurin complex show a composite binding surface with extensive contacts between FK506 and its protein partners as well as between the protein partners themselves (20, 21). We now present a 2.7 Å x-ray structure that shows how rapamycin mediates the heterodimerization of FKBP12 with FRAP.

Binding of FRAP to FKBP12-rapamycin ($K_d = 2$ nM) is mediated by a small domain, the FKBP12-rapamycin-binding (FRB) domain, that can be expressed as a 12-kD soluble protein (22). Crystals (23) of the ternary FKBP12-rapamycin-FRB complex were pre-

pared and the structure was solved (24) by a combination of molecular replacement (MR) with isomorphous replacement for a single anomalously scattering derivative (SIRAS) (Fig. 1, B and C). The resulting MR-SIRAS map was readily interpretable, and the structure was refined to a final *R* factor of 0.193 (8.0 to 2.7 Å data). The ternary complex has a roughly rectangular shape with overall dimensions of 60 Å by 45 Å by 35 Å. The two protein components are virtually the same size, and rapamycin is almost completely buried between them. The ternary complex features an extensive array of rapamycin-protein interactions in two binding pockets lined with aromatic residues. FKBP12 contains a large β sheet composed of five antiparallel β strands (17–19). A short amphipathic α helix is pressed against this sheet, and rapamycin binds in a hydrophobic pocket formed between the α helix and β sheet. Three loops—the 40s loop, which is a bulge in $\beta 5$, the 50s loop connecting $\beta 5$ to α , and the 80s loop connecting $\beta 2$ to $\beta 3$ —surround and contribute to the binding pocket. In general, the structure of the FKBP12-rapamycin portion of the ternary complex does not differ from that of the binary FKBP12-rapamycin complex (18, 19), and the overall root-mean-square deviation between the binary and ternary complex is 1.14 Å for all atoms and 0.49 Å for main chain atoms.

The FRB domain of FRAP forms a four-helix bundle, a common structural motif in globular proteins (25). Its overall dimensions are 30 Å by 45 Å by 30 Å, and all four helices ($\alpha 1$ to $\alpha 4$) have short underhand connections similar to the cytochrome b_{562} fold (26). The NH_2 - and $COOH$ -termini of the FRB domain are close to each other, suggesting that an FRB-type domain could be inserted into other protein chains. The longest helix, $\alpha 3$, has a 60° bend at Tyr²⁰⁷⁴, roughly one-third of the distance from its NH_2 -terminus, and the $\alpha 2$ helix has a small region (Gly²⁰⁴⁹ to Leu²⁰⁵¹) that deviates from a standard α helix. Ignoring the first 10 residues of $\alpha 3$, all four helices are ~26 Å in length and comprise 16 to 19 residues. The $\alpha 1$ and $\alpha 2$ helices are almost parallel (interhelical angle of 22°), as are $\alpha 3$ and $\alpha 4$ (20°), whereas the crossing angles between the $\alpha 1$ - $\alpha 2$ pair and the $\alpha 3$ - $\alpha 4$ pair range from 30° to 60°. The parallel helices are also closer. Helices $\alpha 1$ - $\alpha 2$ and $\alpha 3$ - $\alpha 4$ show the shortest interhelical distances of 6.3 and 7.2 Å, respectively, whereas other closest interhelical contacts range from 10 to 14 Å. Most of the hydrophobic and aromatic residues are located in the interhelical regions, and the hydrophilic residues are exposed to solvent. The first and last helices of the bundle, $\alpha 1$ and $\alpha 4$, form a deep cleft near their crossing point, and this cleft, which is lined by six aromatic side chains, forms the hydrophobic

J. Choi and J. Clardy, Department of Chemistry, Baker Laboratory, Cornell University, Ithaca, NY 14853-1301, USA.

J. Chen and S. L. Schreiber, Howard Hughes Medical Institute and Department of Chemistry and Chemical Biology, Harvard University, Cambridge, MA 02138, USA.

*Present address: Department of Chemistry, Suwon University, Kyunggi 445-773, South Korea.

†To whom correspondence should be addressed.

pocket in which rapamycin binds.

Rapamycin interacts extensively with both FKBP12 and FRB. Its interactions with FKBP12 resemble those described for the binary complex and feature extensive contacts with conserved aromatic residues and five hydrogen bonds (18, 19). Trp⁵⁹ forms the base of the binding pocket and contacts the pipercolinyl ring (C2 to N7)—the most deeply buried portion of rapamycin. A total of 460 Å² (44%) of the solvent-accessible surface area of rapamycin is buried in FKBP12. Rapamycin also interacts with the FRB domain of FRAP through close contacts with aromatic residues, and a series of interactions along the triene arm of rapamycin (C16 to C23) involving Phe²⁰³⁹, Trp²¹⁰¹, Tyr²¹⁰⁵, and Phe²¹⁰⁸ appear especially important (Fig. 2). Ser²⁰³⁵, Leu²⁰³¹, Thr²⁰⁹⁸, Asp²¹⁰², and Tyr²⁰³⁸ also make contact with rapamycin. There are no hydrogen bonds in the FRB-rapamycin interaction, and 340 Å² (33%) of the solvent-accessible surface area of rapamycin participate in the interaction. A small, but important, conformational change in rapamycin is evident between the binary (FKBP12-rapamycin) and ternary (FKBP12-rapamycin-FRB) complexes. In crystal structures of uncomplexed rapamycin (27) and the FKBP12-rapamycin complex (18), the triene arm of rapamycin is planar, with the three double bonds fully conjugated. In the ternary complex, rotations of -15° about C18-C19 and 37° about C20-C21 slightly disrupt the conjugation and move the most deeply buried portion of rapamycin, the methyl group attached to C23, by 1.6 Å (Fig. 1). This conformational alteration of rapamycin avoids a close contact with Phe²¹⁰⁸ and places the deeply buried methyl group in a small crease between Phe²¹⁰⁸ and Leu²⁰³¹ (Fig. 2). The macrocyclic loop of rapamycin is eight carbon atoms larger than the corresponding loop in FK506, and the triene portion of rapamycin reduces the conformational flexibility of the loop and holds it away from the surface of FKBP12—it organizes the loop for binding into a deep pocket. Our analysis suggests that the limited flexibility of the triene arm might also be an important feature of the structure of rapamycin. If FK506 and rapamycin are overlaid, the much shorter loop of FK506 does not approach the binding pocket of the FRB domain of FRAP.

Although rapamycin interacts extensively with both protein partners, the extent to which the proteins interact with each other is relatively limited (Fig. 2). Two regions of the complex show interactions between the proteins: the 40s loop of FKBP12 with $\alpha 4$ of FRB, and the 80s loop of FKBP12 with the $\alpha 1$ - $\alpha 2$ region of FRB. In the 40s- $\alpha 4$ interaction, the OH group of Tyr²¹⁰⁵ and the O atom of Lys⁴⁷ make a short contact and there is also a water-mediated salt bridge. In the other inter-

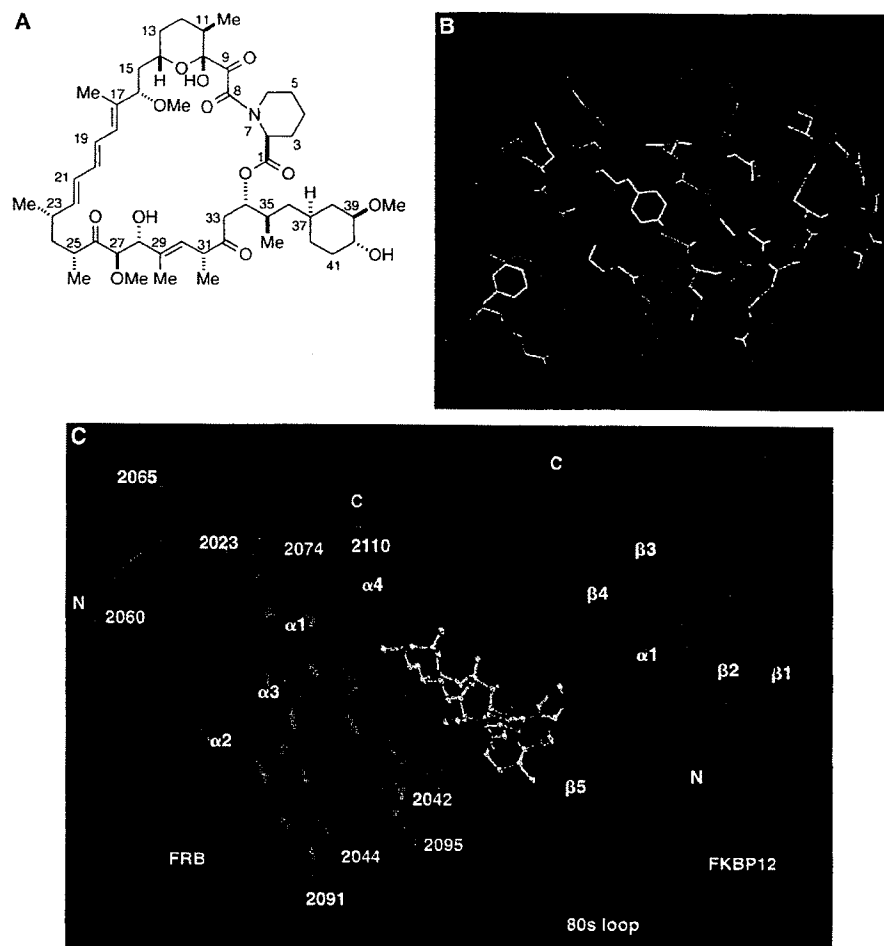


Fig. 1. (A) Chemical structure of rapamycin. (B) The $2F_o - F_c$ electron density of the FRB domain of the FKBP12-rapamycin-FRB complex (24) (F_o , observed structure factor; F_c , calculated structure factor). A model of the final structure is embedded in this initial electron density. (C) Overall structure of the ternary complex between FKBP12 (blue ribbon), rapamycin (ball and stick), and the FRB domain of FRAP (red ribbon). Secondary structural elements are labeled with the conventional numbering scheme for FKBP12. N and C, NH₂- and COOH-termini, respectively. The drawing in (C) was prepared with RIBBONS (31).

action region, the NH₂ group of Arg²⁰⁴² makes short contacts with Oyl of Thr⁸⁵ and the O atom of Gly⁸⁶, and there are two water-mediated interactions. Although the number of interprotein polar interactions is moderate, 400 Å² of solvent-accessible surface area, roughly equivalent to the surface area buried by FKBP12-rapamycin or FRB-rapamycin, participate in the interaction between them. The 80s loop of FKBP12 appears to be one region where the structure of FKBP12 differs between the binary and ternary complexes, with the major change being around Ile⁹⁰, where both side chain and main chain deviations are apparent. These deviations move FKBP12 away from the FRB domain, suggesting repulsion between the proteins in this region.

The residues that form the rapamycin binding pocket of FRAP (Fig. 2) are conserved in yeast Tor1p, Tor2p, and rat RAFT1—other ATM family members that

bind FKBP12-rapamycin—and thus all four proteins are likely to contain a hydrophobic pocket with similar architecture and related function. Overexpression of the Ser¹⁹⁷² (corresponding to Ser²⁰³⁵ of FRAP) → Ile mutant of Tor1p results in marked inhibition of cell growth that is dependent on the kinase activity of the mutant (28). These results indicate that the site bearing the Ser mutation may regulate the neighboring kinase domain of Tor1p (28). The conserved binding pocket associated with a regulatory function suggests that binding of an as yet unidentified ligand may regulate kinase activity. The shape of the binding pocket and the $\alpha 1$ - $\alpha 4$ crossing angle are mutually dependent; thus, ligand binding could result in a change in the crossing angle, and the domain could function as a ligand-dependent conformational switch. FKBP12 might adjust the crossing angle (possibly by having its 80s loop repel the $\alpha 1$ - $\alpha 2$ helical pair of the FRB domain of

REPORTS

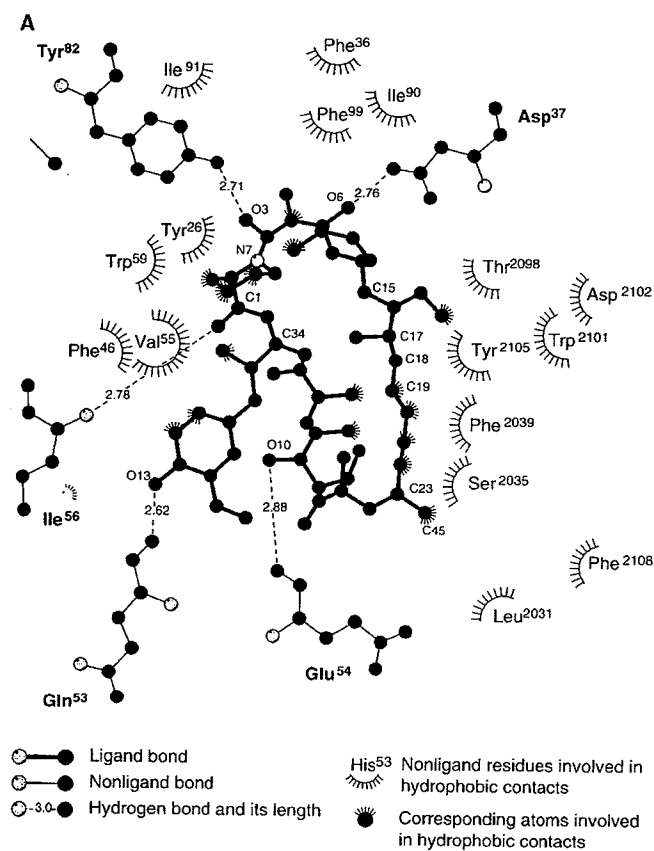
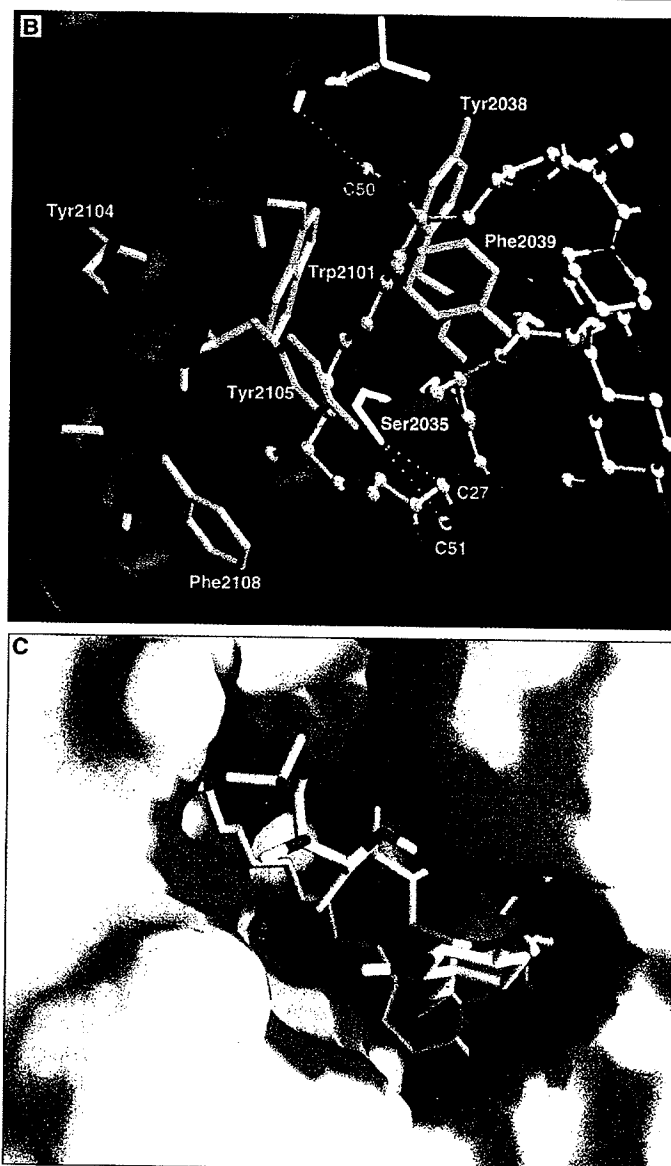


Fig. 2. Interactions of rapamycin with FKBP12 and FRB. (A) A LIGPLOT (32) rendering of the interactions of rapamycin with FKBP12 and FRB. Hydrogen bonds are shown by dashed lines (with lengths in angstroms), and hydrophobic interactions by surface dashes. (B) Close-up of the interactions of rapamycin (ball and stick) with the FRB domain of FRAP (red ribbon). Residue numbering is based on that for FRAP. (C) Complementarity plot of rapamycin with FKBP12 and the FRB domain of FRAP (33). High complementarity is indicated by purple. FKBP12 is on the right and the opening of the deep cavity where the pipecolinyl moiety is buried is visible. The FRB domain of FRAP is on the left, and the most deeply buried methyl group is shown disappearing into the FRB cavity.



FRAP) so that the FRB pocket is optimized for rapamycin binding.

Mutation of Ser²⁰³⁵ to Thr in FRAP renders the protein insensitive to the inhibitory effects of the FKBP12-rapamycin complex; the extra bulk of Thr²⁰³⁵ may prevent binding of rapamycin in the pocket (7) (Fig. 2). Mutations of Trp²¹⁰¹ and Phe²¹⁰⁸ also confer rapamycin resistance (29), and these residues also interact strongly with rapamycin (Fig. 2).

Our data provide a structural framework for understanding the rapamycin-based dimerization of FKBP12 and FRAP. Comparison of the FKBP12-FK506-calciuretin structure (20, 21) with the FKBP12-rapamycin-FRB structure reveals different strategies for the two dimerization modes. Whereas FK506-induced dimerization features extensive protein-

protein interactions, rapamycin-induced dimerization does not. Because rapamycin-induced protein dimerization can form the basis for regulating gene transcription and other cellular processes (30), such structure-based modifications of the interaction might have important practical consequences. The structure also provides insights into structural features and possible regulation of the ATM family of proteins.

REFERENCES AND NOTES

- C. T. Keith and S. L. Schreiber, *Science* **270**, 50 (1995).
- V. A. Zakian, *Cell* **82**, 685 (1995).
- T. Hunter, *ibid.* **83**, 1 (1995).
- S. P. Jackson, *Curr. Biol.* **5**, 1210 (1995).
- E. J. Brown *et al.*, *Nature* **369**, 756 (1994).
- D. Sabatini, H. Erdjument-Bromage, M. Lui, P. Tempst, S. Snyder, *Cell* **78**, 35 (1994).
- E. J. Brown *et al.*, *Nature* **377**, 441 (1995).
- H. Tanaka *et al.*, *J. Am. Chem. Soc.* **109**, 5031 (1987).
- D. C. N. Swindells, P. S. White, J. A. Findlay, *Can. J. Chem.* **56**, 2491 (1978).
- S. N. Sehgal, H. Baker, C. Vezina, *J. Antibiot.* **28**, 727 (1975).
- C. Vezina, A. Kudelski, S. N. Sehgal, *ibid.*, p. 721.
- M. W. Harding, A. Galat, D. E. Uehling, S. L. Schreiber, *Nature* **341**, 758 (1989).
- J. J. Siekerka, S. H. Y. Hung, M. Poe, C. S. Lin, N. H. Sigal, *ibid.*, p. 755.
- S. L. Schreiber, *Science* **251**, 283 (1991).
- J. Liu *et al.*, *Cell* **66**, 807 (1991).
- D. M. Spencer, T. J. Wandless, S. L. Schreiber, G. R. Crabtree, *Science* **262**, 1019 (1993); P. J. Belshaw, S. N. Ho, G. R. Crabtree, *Proc. Natl. Acad. Sci. U.S.A.* **93**, 4604 (1996).
- G. D. Van Duyne, R. F. Standaert, P. A. Karpus, S. L. Schreiber, J. Clardy, *Science* **251**, 839 (1991).
- G. D. Van Duyne, R. F. Standaert, S. L. Schreiber, J. Clardy, *J. Am. Chem. Soc.* **113**, 7433 (1991).
- G. D. Van Duyne, R. F. Standaert, P. A. Karpus, S. L. Schreiber, J. Clardy, *J. Mol. Biol.* **229**, 105 (1993).
- C. R. Kissinger *et al.*, *Nature* **378**, 541 (1995).
- J. P. Griffith *et al.*, *Cell* **82**, 507 (1995).
- J. Chen, X. F. Zheng, E. J. Brown, S. L. Schreiber,

Proc. Natl. Acad. Sci. U.S.A. 92, 4947 (1995).

23. The expression and purification of recombinant human FKBP12 (79) and the FRB domain of human FRAP (22) have been described. Crystals of FKBP12-rapamycin-FRB were grown in 2 to 3 weeks at room temperature from hanging drops prepared from FKBP12 [10 mg/ml, in 10 mM tris-HCl (pH 8.0)], two equivalents of rapamycin (in methanol), and one equivalent of FRB [10 mg/ml, in 50 mM tris-HCl (pH 8.0)]. The well solution contained 20% (w/v) polyethylene glycol 8000, 10% methypentanediol, and 10 mM tris-HCl (pH 8.5). The rod-shaped crystals are orthorhombic, space group $P2_12_12_1$, with cell constants $a = 44.63$, $b = 52.14$, and $c = 102.53$ Å, and contain one ternary complex in the asymmetrical unit.
24. Data to a resolution of 2.7 Å (43,447 measurements of 6920 unique reflections, 98.5% complete, $R_{\text{sym}} = 0.071$) were collected from a crystal of dimensions 0.3 mm by 0.2 mm by 0.1 mm with the use of a San Diego multiwire area detector on a Rigaku RU-200 rotating anode x-ray source. Experimental phases were obtained from MR and SIRAS. MR with X-PLOR [A. T. Brünger, J. Kuriyan, M. Karplus, *Science* 235, 458 (1987)] and the FKBP12-rapamycin model (19) yielded a clear solution, but the resulting electron density map was noisy. A mercury derivative was prepared (2 mM HgCl_2 , overnight), and the two heavy atom sites were refined with PHASES [W. Furey and S. Swaminathan, *ACA Abstr.* 18, 73 (1990)]. Anomalous dispersion measurements were included in this data set and 16 cycles of solvent flattening were applied (PHASES). The resulting electron density map clearly showed the four-helix-bundle architecture of FRB. The FKBP12-rapamycin portion of the structure was well defined in the initial electron density map, and minor changes in the backbone of the 30s loop and some side chains were sufficient to fit the model. For the FRB portion, most of a polyaniline chain could be traced for the helical regions of the initial map. After several cycles of positional refinement (X-PLOR), loop regions could also be traced and the side chains assigned. CHAIN [J. S. Sack, *J. Mol. Graphics* 6, 244 (1988)] was used for model fitting and building the structure. A total of 95 residues in the FRB domain of FRAP (three residues in the NH_2 -terminal and two residues in the COOH -terminal regions showed no electron density and were not included), all residues of FKBP12, all atoms of rapamycin, and 23 water molecules were included in the final model. FRB residues are numbered according to FRAP numbering. The current R factor is 0.193 ($R_{\text{free}} = 0.299$) for data from 8 to 2.7 Å. The root-mean-square deviations of bond lengths and bond angles are 0.008 Å and 1.48°, respectively. The average temperature factors for all atoms and main chain atoms are 17.0 and 14.7 Å², respectively.
25. N. L. Harris, S. R. Presnell, F. E. Cohen, *J. Mol. Biol.* 236, 1356 (1994).
26. F. Lederer, A. Glatigny, P. H. Bethge, H. D. Bellamy, F. S. Mathews, *ibid.* 148, 427 (1981).
27. J. A. Findlay and L. Radics, *Can. J. Chem.* 58, 579 (1980).
28. X. F. Zheng, D. Fiorentino, J. Chen, G. R. Crabtree, S. L. Schreiber, *Cell* 82, 121 (1995).
29. M. C. Lorenz and J. Heitman, *J. Biol. Chem.* 270, 27531 (1995).
30. V. M. Rivera et al., *Nature Med.*, in press.
31. M. Carson, *J. Mol. Graphics* 5, 103 (1987).
32. A. C. Wallace, R. A. Laskowski, J. M. Thornton, *Prot. Engin.* 8, 127 (1995).
33. A. Nicholls, K. Sharp, B. Honig, *GRASP Manual* (Columbia Univ. Press, New York, 1992).
34. We thank S. Ealick, J. Liang, and R. Gillilan for discussions. The Cornell work was funded in part by USPHS grant CA59021 (to J.C.) and the Harvard work by an Irvington Institute Fellowship (to J.C.) and USPHS grant GM38625 (to S.L.S.). S.L.S. is a Howard Hughes Medical Institute Investigator. Atomic coordinates have been deposited in the Protein Data Bank under the accession number 1FAP.

15 March 1996; accepted 15 May 1996

Long-Term Lymphohematopoietic Reconstitution by a Single CD34-Low/Negative Hematopoietic Stem Cell

Masatake Osawa,* Ken-ichi Hanada, Hirofumi Hamada, Hiromitsu Nakauchi†

Hematopoietic stem cells (HSCs) supply all blood cells throughout life by making use of their self-renewal and multilineage differentiation capabilities. A monoclonal antibody raised to the mouse homolog of CD34 (mCD34) was used to purify mouse HSCs to near homogeneity. Unlike in humans, primitive adult mouse bone marrow HSCs were detected in the mCD34 low to negative fraction. Injection of a single mCD34^{low/-}, c-Kit⁺, Sca-1⁺, lineage markers negative (Lin⁻) cell resulted in long-term reconstitution of the lymphohematopoietic system in 21 percent of recipients. Thus, the purified HSC population should enable analysis of the self-renewal and multilineage differentiation of individual HSCs.

CD34 is a marker of human HSCs, and all colony-forming activity of human bone marrow (BM) cells is found in the CD34-positive fraction (1). Clinical transplantation studies that used enriched CD34⁺ BM cells also indicated the presence of HSCs with long-term BM reconstitution ability within this fraction (2). After isolation of the human CD34 gene, the mouse homolog (mCD34) was isolated by cross-hybridization (3). To examine the expression and function of mCD34, we raised a monoclonal antibody (mAb), 49E8 [rat immunoglobulin G2a (IgG2a)], to mCD34 by immunizing rats with a glutathione-S-transferase (GST)-mCD34 fusion protein. This mAb stained BaF3 cells transfected with a full-length mCD34 cDNA but not mock-transfected cells (4). Murine cell lines such as PA6, NIH 3T3, M1, and DA1, shown by reverse transcriptase-polymerase chain reaction (RT-PCR) to contain mCD34 mRNA, were also stained by this mAb, indicating that 49E8, although specific for a GST-mCD34 fusion protein, could also recognize the native form of mCD34 as expressed on various cell types (4).

We next examined adult mouse BM for expression of mCD34. Four-color fluorescence-activated cell sorter (FACS) analysis was done after sequential staining of BM cells with a combination of lineage-specific mAbs to CD4, CD8, B220, Gr-1, Mac-1, and TER119, and then a mixture of mAbs to c-Kit (ACK-2), Ly6A/E (Sca-1), and mCD34 (5).

M. Osawa and H. Nakauchi, Department of Immunology, Institute of Basic Medical Sciences and Center for Tsukuba Advanced Research Alliance, University of Tsukuba, Tsukuba Science-City, Ibaraki 305, Japan. K.-i. Hanada and H. Hamada, Department of Molecular Biotherapy, Cancer Chemotherapy Center, Japanese Foundation for Cancer Research, Tokyo 170, Japan.

*Present address: KIRIN Pharmaceutical Research Laboratory, Gunma 371, Japan.

†To whom correspondence should be addressed.

Monoclonal antibody 49E8 reacted with $2.5 \pm 0.5\%$ (mean \pm SD) of total BM cells, with most of the positive cells occurring in the Lin⁻ fraction (Fig. 1A). More than 90% of the c-Kit⁺ Sca-1⁺ Lin⁻ cells previously shown to contain primitive HSCs (6) stained brightly with 49E8, whereas the remainder were low to negative (Fig. 1B). The frequency of mCD34⁺ c-Kit⁺ Sca-1⁺ Lin⁻ cells and mCD34⁻ c-Kit⁺ Sca-1⁺ Lin⁻ cells among total nucleated BM cells was $0.073 \pm 0.028\%$ (mean \pm SD, $n = 5$) and $0.004 \pm 0.003\%$ (mean \pm SD, $n = 5$), respectively.

To determine whether mouse HSCs express mCD34, we sorted subpopulations by FACS and examined their stem cell activity. Within the c-Kit⁺ Sca-1⁺ Lin⁻ population, the frequency of interleukin-3 (IL-3)-dependent colony-forming unit culture (CFU-C) per 200 cells was $20.0 \pm 3.9\%$ (mean \pm SD, $n = 8$) (7) for mCD34⁺ cells but only $0.16 \pm 0.4\%$ (mean \pm SD, $n = 8$) in the CD34⁻ fraction. Similarly, mCD34⁺ cells contained $14.1 \pm 3.4\%$ (mean \pm SD, $n = 15$) day 12 CFU spleen (CFU-S) per 200 cells, whereas in the mCD34⁻ fraction this value was $1.6 \pm 1.7\%$ (mean \pm SD, $n = 15$) (8). Thus, colony-forming activity was positively correlated with mCD34 expression among c-Kit⁺ Sca-1⁺ Lin⁻ cells. When these cells were cultured in the presence of both IL-3 and stem cell factor (SCF), however, 80% of mCD34⁺ c-Kit⁺ Sca-1⁺ Lin⁻ cells formed large multilineage colonies (7).

For in vivo analyses, c-Kit⁺ Sca-1⁺ Lin⁻ cells were fractionated into mCD34^{low/-} (Fr. 1), mCD34⁺ (Fr. 2), and CD34⁺ (Fr. 3) subpopulations according to their mCD34 expression by FACS (Fig. 2A). Although 100 c-Kit⁺ Sca-1⁺ Lin⁻ cells were sufficient to radioprotect a lethally irradiated mouse, injection of 300 cells from either the Fr. 1 or Fr. 3 subpopulation (Fig. 2A) alone showed poor radioprotective ability (9). When cells

REPORTS

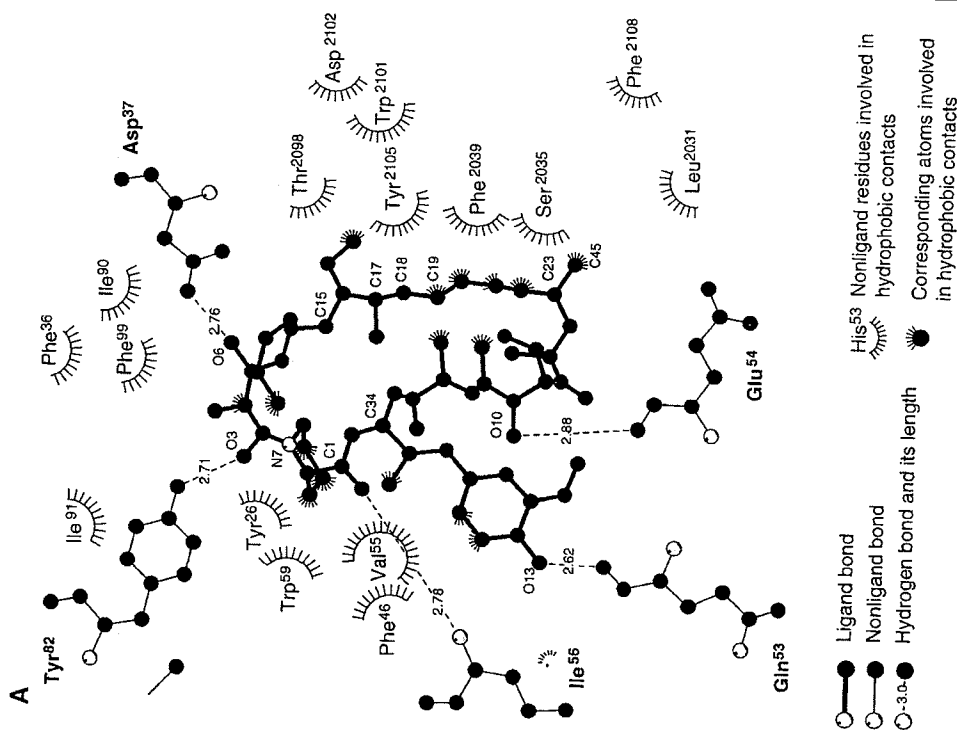


Fig. 2. Interactions of rapamycin with FKBP12 and FRB. **(A)** A LIGPLOT (32) rendering of the interactions of rapamycin with FKBP12 and FRB. Hydrogen bonds are shown by dashed lines (with lengths in angstroms), and hydrophobic interactions by surface dashes. **(B)** Close-up of the interactions of rapamycin (ball and stick) with the FRB domain of FRAP (red ribbon). Residue numbering is based on that for FRAP. **(C)** Complementarity plot of rapamycin with FKBP12 and the FRB domain of FRAP (33). High complementarity is indicated by purple. FKBP12 is on the right and the opening of the deep cavity where the piperidyl moiety is buried is visible. The FRB domain of FRAP is on the left, and the most deeply buried methyl group is shown disappearing into the FRB cavity.

FRAP) so that the FRB pocket is optimized for rapamycin binding.

protein interactions, rapamycin-induced dimerization does not. Because rapamycin-

8. H. Tanaka et al., *J. Am. Chem. Soc.* 109, 5031 (1987).

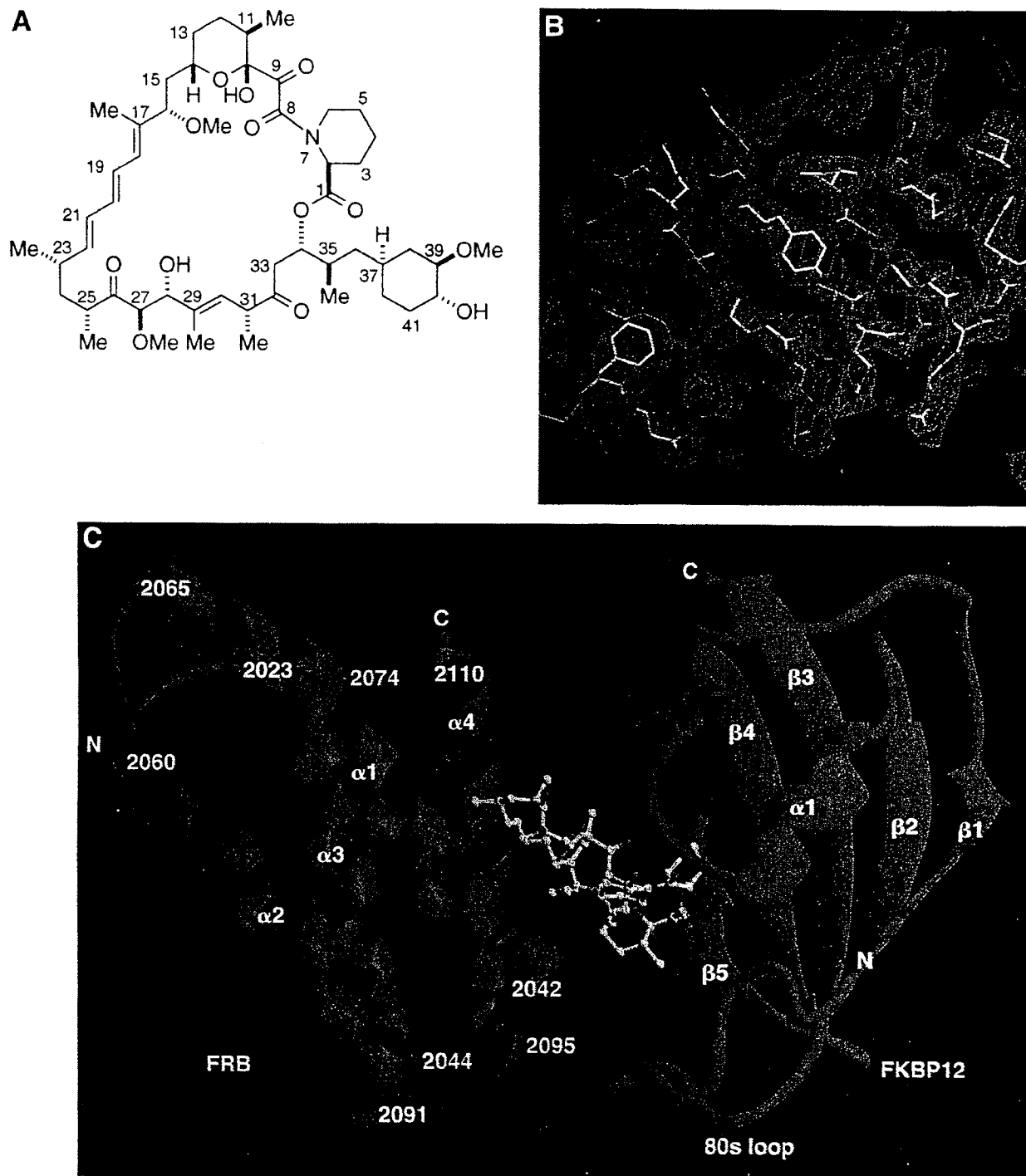


Fig. 1. (A) Chemical structure of rapamycin. **(B)** The $2F_o - F_c$ electron density of the FRB domain of the FKBP12-rapamycin-FRB complex (24) (F_o , observed structure factor; F_c , calculated structure factor). A model of the final structure is embedded in this initial electron density. **(C)** Overall structure of the ternary complex between FKBP12 (blue ribbon), rapamycin (ball and stick), and the FRB domain of FRAP (red ribbon). Secondary structural elements are labeled with the conventional numbering scheme for FKBP12. N and C, NH_2 - and COOH -termini, respectively. The drawing in (C) was prepared with RIBBONS (31).

action region, the NH_2 group of Arg²⁰⁴² makes short contacts with O γ 1 of Thr⁸⁵ and the O atom of Gly⁸⁶, and there are two water-

bind FKBP12-rapamycin—and thus all four proteins are likely to contain a hydrophobic pocket with similar architecture and related

ISSN 0036-8075
12 JULY 1996
VOLUME 273
NUMBER 5272

SCIENCE



AMERICAN
ASSOCIATION FOR THE
ADVANCEMENT OF
SCIENCE

NEWS

The Decline of German Universities	172
Foreign Students Bypassing Germany	173
Disputed Results Now Just a Footnote	174
Panel Backs Joint Bion Mission	175
Earmark for New Ship Puts Academics Over Pork Barrel	176
Italian Bioethics: Embryo Report Opens Old Wounds	177
Publisher Draws Censorship Charge	177
Tobacco Studies: UC Objects to Research Restrictions	178
Silver Thread Boosts Current Capacity	178
Unruly Sun Emerges in Solar Observatory's First Results	179
Spying On the Sun—on the Cheap	180
Evolutionary and Systematic Biologists Converge	181
Twinkle, Twinkle, Little Quasar	182

Protein Matchmaker May Lead New Gene Therapy to the Altar	183
---	-----

SPECIAL NEWS REPORT

Putting Prions to the Test	184
Flipping Yeast	186
Prusiner and the Press	188

PERSPECTIVES

If a Tree Falls in the Forest...	201
M. Keller, D. A. Clark, D. B. Clark, A. M. Weitz, E. Veldkamp	

The Shrewd Grasp of RNA Polymerase	202
R. Landick and J. W. Roberts	

Rho Returns: Its Targets in Focal Adhesions	203
H. Bussey	

ARTICLE

New Designs of Macroporous Polymers and Supports: From Separation to Biocatalysis	205
F. Svec and J. M. J. Fréchet	

184

Do prions mangle proteins?

DEPARTMENTS

THIS WEEK IN SCIENCE	157
EDITORIAL	163
Scientific Imagination and Integrity	
K. J. Ryan	
LETTERS	165
Not the "Dark Ages": W. C. Barker and R. S. Ledley	
• Dinosaurs and Their Youth: M. A. Norell and J. M. Clark; N. R. Geist and T. D. Jones • Tobacco Research: J. F. Glenn; J. Cohen; T. D. Sterling • Uninterrupted Electric Power: D. N. Baker and J. G. Kappenman	
SCIENCESCOPE	171

RANDOM SAMPLES	191
High Court Won't Review <i>Hopwood</i> • Manatee Killer Revealed • Canada Considers Gene Law	
BOOK REVIEWS	196
<i>Bendectin and Birth Defects</i> , reviewed by S. Bartlett Foote • <i>The Mismeasure of Man</i> • <i>The World According to Wavelets</i> • <i>Wavelets</i> • Vignette • Books Received	
PRODUCTS & MATERIALS	262
SCIENCE'S NEXT WAVE	265
Bioinformatics: New Frontier Calls Young Scientists	

AAAS Board of Directors

Rita R. Colwell
Retiring President, Chairman
Jane Lubchenco
President
Mildred S. Dresselhaus
President-elect

Sheila Jasanoff
William A. Lester Jr.
Simon A. Levin
Marcia C. Linn
Michael J. Novacek
Anna C. Roosevelt
Jean E. Taylor
Nancy S. Wexler

William T. Golden
Treasurer
Richard S. Nicholson
Executive Officer

■ SCIENCE (ISSN 0036-8075) is published weekly on Friday, except the last week in December, by the American Association for the Advancement of Science, 1200 New York Avenue, NW, Washington, DC 20005. Periodicals Mail postage (publication No. 484460) paid at Washington, DC, and additional mailing offices. Copyright © 1996 by the American Association for the Advancement of Science. The title SCIENCE is a registered trademark of the AAAS. Domestic individual membership and subscription (51 issues): \$102 (\$55 allocated to subscription). Domestic institutional subscription (51 issues): \$250. Foreign postage extra: Mexico, Caribbean (surface mail) \$55; other countries (air assist delivery) \$90. First class, airmail, student, and emeritus rates on request. Canadian rates with GST available upon request, GST #1254 88122. Printed in the U.S.A.

Structure of the FKBP12-Rapamycin Complex Interacting with the Binding Domain of Human FRAP

Jungwon Choi,* Jie Chen, Stuart L. Schreiber, Jon Clardy†

Rapamycin, a potent immunosuppressive agent, binds two proteins: the FK506-binding protein (FKBP12) and the FKBP-rapamycin-associated protein (FRAP). A crystal structure of the ternary complex of human FKBP12, rapamycin, and the FKBP12-rapamycin-binding (FRB) domain of human FRAP at a resolution of 2.7 angstroms revealed the two proteins bound together as a result of the ability of rapamycin to occupy two different hydrophobic binding pockets simultaneously. The structure shows extensive interactions between rapamycin and both proteins, but fewer interactions between the proteins. The structure of the FRB domain of FRAP clarifies both rapamycin-independent and -dependent effects observed for mutants of FRAP and its homologs in the family of proteins related to the ataxia-telangiectasia mutant gene product, and it illustrates how a small cell-permeable molecule can mediate protein dimerization.

A dividing cell must pass various checkpoints as it proceeds through the cell cycle, and error-free division requires the ability to rectify DNA lesions (1, 2). The ataxia-telangiectasia mutant (ATM) gene product, the catalytic subunit of the DNA-dependent protein kinase, and the products of yeast genes such as *TOR1*, *TOR2*, and *MEC1* (*ESR1*) are members of a family of large molecular size proteins that participate in cell cycle progression and checkpoints as well as in DNA repair and recombination (1–4). All members of the ATM family contain a COOH-terminal kinase domain (1–4), but no structural information is available for any domain of any family member. Human FRAP (rat RAFT), one member of this family, is a 289-kD protein that binds FKBP12-rapamycin, regulates p70 ribosomal protein S6 kinase, and is required for G_1 cell cycle progression in several cell types (5–7).

The potent immunosuppressive agents FK506 (8) and rapamycin (9–11) (Fig. 1A) share the same cellular target: the 12-kD FK506-binding protein, FKBP12 (12, 13). Although both rapamycin and FK506 bind to FKBP12 with high affinity [dissociation constant (K_d), 0.2 to 0.4 nM], they effect immunosuppression through different mechanisms. Whereas FK506 interrupts the signal from the T cell receptor, rapamycin interrupts the signal from the interleukin-2 receptor and the receptors for other cytokines and growth factors (14). Binding of similar molecules, such as FK506 and rapamycin,

to the same protein can disrupt different signals because the protein-ligand complexes, (not the individual components) are the active entities (14). FKBP12-FK506 inhibits calcineurin, a serine-threonine phosphatase (15), whereas FKBP12-rapamycin binds to FRAP (5). Thus, small cell-permeable molecules can induce proteins to associate in a manner similar to that by which growth factors (such as human growth hormone), cytokines (such as interleukin-2), and intracellular signaling proteins (such as GRB2) induce dimerization of signaling proteins. These naturally occurring inducers of dimerization have inspired the design of synthetic molecules that induce dimerization of intracellular proteins and result in the activation of cytoplasmic signaling pathways (16).

FK506 and rapamycin bind FKBP12 in a hydrophobic pocket, and an important feature of both FKBP12-ligand structures is the large fraction, ~50%, of ligand exposed on the exterior of the complex (17–19). A composite surface—a surface with contributions from both ligand (FK506 or rapamycin) and the protein (FKBP12)—mediates the interaction of the FKBP12-ligand complex with its target (14). Two independent x-ray structures of the ternary FKBP12-FK506-calcineurin complex show a composite binding surface with extensive contacts between FK506 and its protein partners as well as between the protein partners themselves (20, 21). We now present a 2.7 Å x-ray structure that shows how rapamycin mediates the heterodimerization of FKBP12 with FRAP.

Binding of FRAP to FKBP12-rapamycin ($K_d = 2$ nM) is mediated by a small domain, the FKBP12-rapamycin-binding (FRB) domain, that can be expressed as a 12-kD soluble protein (22). Crystals (23) of the ternary FKBP12-rapamycin-FRB complex were pre-

pared and the structure was solved (24) by a combination of molecular replacement (MR) with isomorphous replacement for a single anomalously scattering derivative (SIRAS) (Fig. 1, B and C). The resulting MR-SIRAS map was readily interpretable, and the structure was refined to a final *R* factor of 0.193 (8.0 to 2.7 Å data). The ternary complex has a roughly rectangular shape with overall dimensions of 60 Å by 45 Å by 35 Å. The two protein components are virtually the same size, and rapamycin is almost completely buried between them. The ternary complex features an extensive array of rapamycin-protein interactions in two binding pockets lined with aromatic residues. FKBP12 contains a large β sheet composed of five antiparallel β strands (17–19). A short amphipathic α helix is pressed against this sheet, and rapamycin binds in a hydrophobic pocket formed between the α helix and β sheet. Three loops—the 40s loop, which is a bulge in β_5 , the 50s loop connecting β_5 to α , and the 80s loop connecting β_2 to β_3 —surround and contribute to the binding pocket. In general, the structure of the FKBP12-rapamycin portion of the ternary complex does not differ from that of the binary FKBP12-rapamycin complex (18, 19), and the overall root-mean-square deviation between the binary and ternary complex is 1.14 Å for all atoms and 0.49 Å for main chain atoms.

The FRB domain of FRAP forms a four-helix bundle, a common structural motif in globular proteins (25). Its overall dimensions are 30 Å by 45 Å by 30 Å, and all four helices (α_1 to α_4) have short underhand connections similar to the cytochrome b_5 fold (26). The NH_2 - and $COOH$ -termini of the FRB domain are close to each other, suggesting that an FRB-type domain could be inserted into other protein chains. The longest helix, α_3 , has a 60° bend at Tyr²⁰⁷⁴, roughly one-third of the distance from its NH_2 -terminus, and the α_2 helix has a small region (Gly²⁰⁴⁹ to Leu²⁰⁵¹) that deviates from a standard α helix. Ignoring the first 10 residues of α_3 , all four helices are ~26 Å in length and comprise 16 to 19 residues. The α_1 and α_2 helices are almost parallel (interhelical angle of 22°), as are α_3 and α_4 (20°), whereas the crossing angles between the α_1 - α_2 pair and the α_3 - α_4 pair range from 30° to 60°. The parallel helices are also closer. Helices α_1 - α_2 and α_3 - α_4 show the shortest interhelical distances of 6.3 and 7.2 Å, respectively, whereas other closest interhelical contacts range from 10 to 14 Å. Most of the hydrophobic and aromatic residues are located in the interhelical regions, and the hydrophilic residues are exposed to solvent. The first and last helices of the bundle, α_1 and α_4 , form a deep cleft near their crossing point, and this cleft, which is lined by six aromatic side chains, forms the hydrophobic

J. Choi and J. Clardy, Department of Chemistry, Baker Laboratory, Cornell University, Ithaca, NY 14853-1301, USA.

J. Chen and S. L. Schreiber, Howard Hughes Medical Institute and Department of Chemistry and Chemical Biology, Harvard University, Cambridge, MA 02138, USA.

*Present address: Department of Chemistry, Suwon University, Kyunggi 445-773, South Korea.

†To whom correspondence should be addressed.

pocket in which rapamycin binds.

Rapamycin interacts extensively with both FKBP12 and FRB. Its interactions with FKBP12 resemble those described for the binary complex and feature extensive contacts with conserved aromatic residues and five hydrogen bonds (18, 19). Trp⁵⁹ forms the base of the binding pocket and contacts the pipercolinyl ring (C2 to N7)—the most deeply buried portion of rapamycin. A total of 460 Å² (44%) of the solvent-accessible surface area of rapamycin is buried in FKBP12. Rapamycin also interacts with the FRB domain of FRAP through close contacts with aromatic residues, and a series of interactions along the triene arm of rapamycin (C16 to C23) involving Phe²⁰³⁹, Trp²¹⁰¹, Tyr²¹⁰⁵, and Phe²¹⁰⁸ appear especially important (Fig. 2). Ser²⁰³⁵, Leu²⁰⁴¹, Thr²⁰⁹⁸, Asp²¹⁰², and Tyr²⁰⁴⁸ also make contact with rapamycin. There are no hydrogen bonds in the FRB-rapamycin interaction, and 340 Å² (33%) of the solvent-accessible surface area of rapamycin participate in the interaction. A small, but important, conformational change in rapamycin is evident between the binary (FKBP12-rapamycin) and ternary (FKBP12-rapamycin-FRB) complexes. In crystal structures of uncomplexed rapamycin (27) and the FKBP12-rapamycin complex (18), the triene arm of rapamycin is planar, with the three double bonds fully conjugated. In the ternary complex, rotations of -15° about C18-C19 and 37° about C20-C21 slightly disrupt the conjugation and move the most deeply buried portion of rapamycin, the methyl group attached to C23, by 1.6 Å (Fig. 1). This conformational alteration of rapamycin avoids a close contact with Phe²¹⁰⁸ and places the deeply buried methyl group in a small crease between Phe²¹⁰⁸ and Leu²⁰³¹ (Fig. 2). The macrocyclic loop of rapamycin is eight carbon atoms larger than the corresponding loop in FK506, and the triene portion of rapamycin reduces the conformational flexibility of the loop and holds it away from the surface of FKBP12—it organizes the loop for binding into a deep pocket. Our analysis suggests that the limited flexibility of the triene arm might also be an important feature of the structure of rapamycin. If FK506 and rapamycin are overlaid, the much shorter loop of FK506 does not approach the binding pocket of the FRB domain of FRAP.

Although rapamycin interacts extensively with both protein partners, the extent to which the proteins interact with each other is relatively limited (Fig. 2). Two regions of the complex show interactions between the proteins: the 40s loop of FKBP12 with $\alpha 4$ of FRB, and the 80s loop of FKBP12 with the $\alpha 1$ - $\alpha 2$ region of FRB. In the 40s- $\alpha 4$ interaction, the OH group of Tyr²¹⁰⁵ and the O atom of Lys⁴⁷ make a short contact and there is also a water-mediated salt bridge. In the other inter-

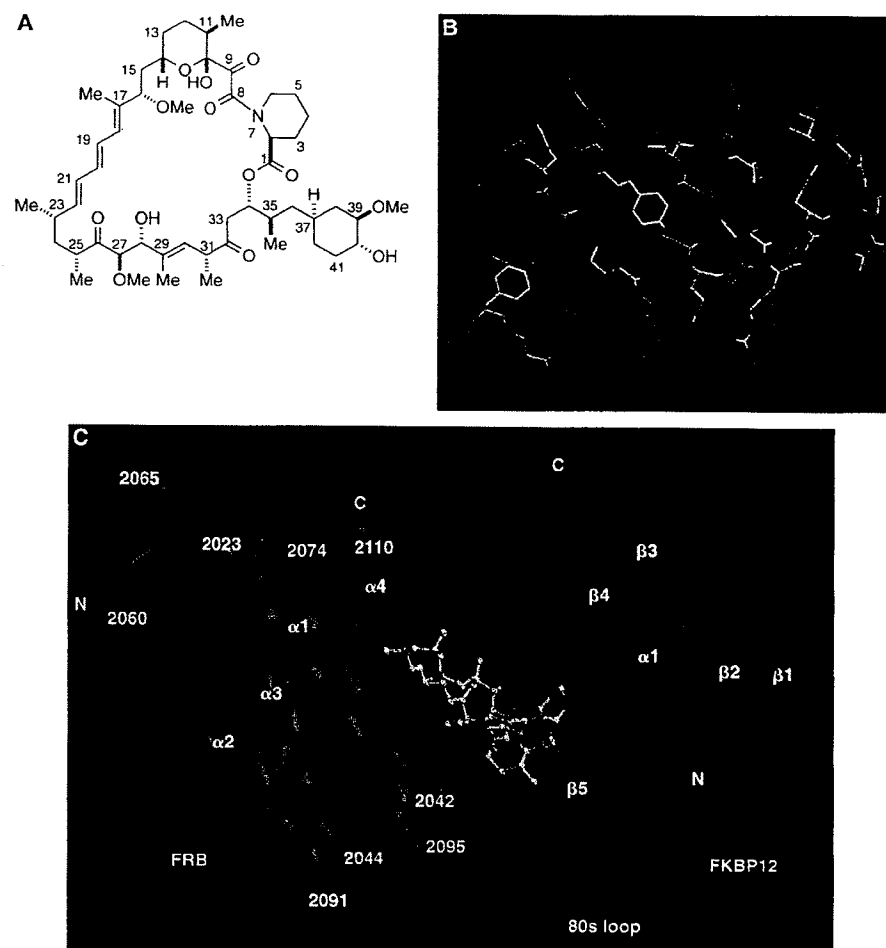


Fig. 1. (A) Chemical structure of rapamycin. (B) The $2F_o - F_c$ electron density of the FRB domain of the FKBP12-rapamycin-FRB complex (24) (F_o , observed structure factor; F_c , calculated structure factor). A model of the final structure is embedded in this initial electron density. (C) Overall structure of the ternary complex between FKBP12 (blue ribbon), rapamycin (ball and stick), and the FRB domain of FRAP (red ribbon). Secondary structural elements are labeled with the conventional numbering scheme for FKBP12. N and C, NH₂- and COOH-termini, respectively. The drawing in (C) was prepared with RIBBONS (31).

action region, the NH₂ group of Arg²⁰⁴² makes short contacts with Oyl of Thr⁸⁵ and the O atom of Gly⁸⁶, and there are two water-mediated interactions. Although the number of interprotein polar interactions is moderate, 400 Å² of solvent-accessible surface area, roughly equivalent to the surface area buried by FKBP12-rapamycin or FRB-rapamycin, participate in the interaction between them. The 80s loop of FKBP12 appears to be one region where the structure of FKBP12 differs between the binary and ternary complexes, with the major change being around Ile⁹⁰, where both side chain and main chain deviations are apparent. These deviations move FKBP12 away from the FRB domain, suggesting repulsion between the proteins in this region.

The residues that form the rapamycin binding pocket of FRAP (Fig. 2) are conserved in yeast Tor1p, Tor2p, and rat RAFT1—other ATM family members that

bind FKBP12-rapamycin—and thus all four proteins are likely to contain a hydrophobic pocket with similar architecture and related function. Overexpression of the Ser¹⁹⁷² (corresponding to Ser²⁰³⁵ of FRAP) → Ile mutant of Tor1p results in marked inhibition of cell growth that is dependent on the kinase activity of the mutant (28). These results indicate that the site bearing the Ser mutation may regulate the neighboring kinase domain of Tor1p (28). The conserved binding pocket associated with a regulatory function suggests that binding of an as yet unidentified ligand may regulate kinase activity. The shape of the binding pocket and the $\alpha 1$ - $\alpha 4$ crossing angle are mutually dependent; thus, ligand binding could result in a change in the crossing angle, and the domain could function as a ligand-dependent conformational switch. FKBP12 might adjust the crossing angle (possibly by having its 80s loop repel the $\alpha 1$ - $\alpha 2$ helical pair of the FRB domain of

REPORTS

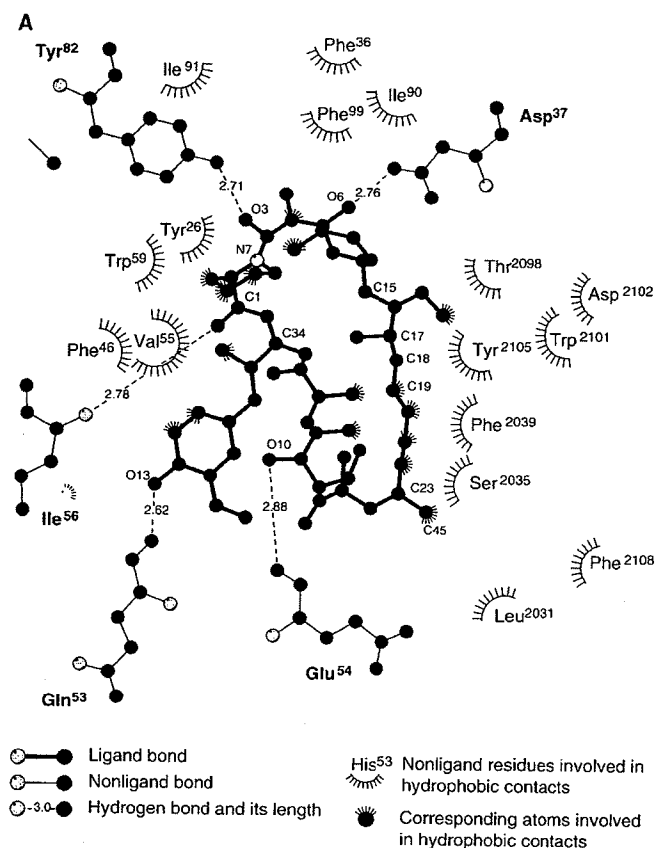
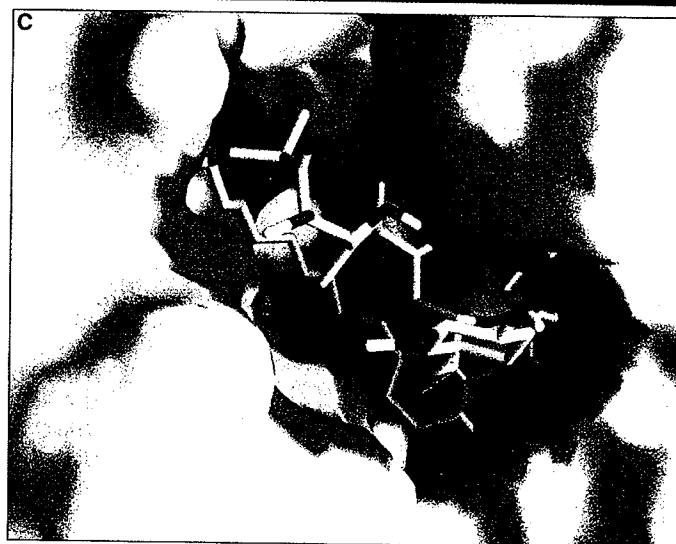
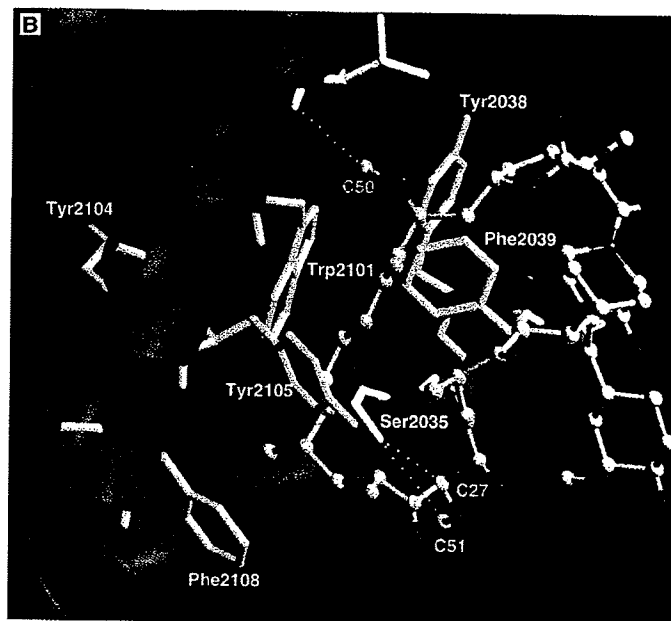


Fig. 2. Interactions of rapamycin with FKBP12 and FRB. (A) A LIGPLOT (32) rendering of the interactions of rapamycin with FKBP12 and FRB. Hydrogen bonds are shown by dashed lines (with lengths in angstroms), and hydrophobic interactions by surface dashes. (B) Close-up of the interactions of rapamycin (ball and stick) with the FRB domain of FRAP (red ribbon). Residue numbering is based on that for FRAP. (C) Complementarity plot of rapamycin with FKBP12 and the FRB domain of FRAP (33). High complementarity is indicated by purple. FKBP12 is on the right and the opening of the deep cavity where the pipecolinyl moiety is buried is visible. The FRB domain of FRAP is on the left, and the most deeply buried methyl group is shown disappearing into the FRB cavity.



FRAP) so that the FRB pocket is optimized for rapamycin binding.

Mutation of Ser²⁰³⁵ to Thr in FRAP renders the protein insensitive to the inhibitory effects of the FKBP12-rapamycin complex; the extra bulk of Thr²⁰³⁵ may prevent binding of rapamycin in the pocket (7) (Fig. 2). Mutations of Trp²¹⁰¹ and Phe²¹⁰⁸ also confer rapamycin resistance (29), and these residues also interact strongly with rapamycin (Fig. 2).

Our data provide a structural framework for understanding the rapamycin-based dimerization of FKBP12 and FRAP. Comparison of the FKBP12-FK506-calciuretin structure (20, 21) with the FKBP12-rapamycin-FRB structure reveals different strategies for the two dimerization modes. Whereas FK506-induced dimerization features extensive protein-

protein interactions, rapamycin-induced dimerization does not. Because rapamycin-induced protein dimerization can form the basis for regulating gene transcription and other cellular processes (30), such structure-based modifications of the interaction might have important practical consequences. The structure also provides insights into structural features and possible regulation of the ATM family of proteins.

REFERENCES AND NOTES

- C. T. Keith and S. L. Schreiber, *Science* **270**, 50 (1995).
- V. A. Zakian, *Cell* **82**, 685 (1995).
- T. Hunter, *ibid.* **83**, 1 (1995).
- S. P. Jackson, *Curr. Biol.* **5**, 1210 (1995).
- E. J. Brown *et al.*, *Nature* **369**, 756 (1994).
- D. Sabatini, H. Erdjument-Bromage, M. Lui, P. Tempst, S. Snyder, *Cell* **78**, 35 (1994).
- E. J. Brown *et al.*, *Nature* **377**, 441 (1995).
- H. Tanaka *et al.*, *J. Am. Chem. Soc.* **109**, 5031 (1987).
- D. C. N. Swindells, P. S. White, J. A. Findlay, *Can. J. Chem.* **56**, 2491 (1978).
- S. N. Sehgal, H. Baker, C. Vezina, *J. Antibiot.* **28**, 727 (1975).
- C. Vezina, A. Kudelski, S. N. Sehgal, *ibid.*, p. 721.
- M. W. Harding, A. Galat, D. E. Uehling, S. L. Schreiber, *Nature* **341**, 758 (1989).
- J. J. Siekierka, S. H. Y. Hung, M. Poe, C. S. Lin, N. H. Sigal, *ibid.*, p. 755.
- S. L. Schreiber, *Science* **251**, 283 (1991).
- J. Liu *et al.*, *Cell* **66**, 807 (1991).
- D. M. Spencer, T. J. Wandless, S. L. Schreiber, G. R. Crabtree, *Science* **262**, 1019 (1993); P. J. Belshaw, S. N. Ho, G. R. Crabtree, *Proc. Natl. Acad. Sci. U.S.A.* **93**, 4604 (1996).
- G. D. Van Duyn, R. F. Standaert, P. A. Karplus, S. L. Schreiber, J. Clardy, *Science* **251**, 839 (1991).
- G. D. Van Duyn, R. F. Standaert, S. L. Schreiber, J. Clardy, *J. Am. Chem. Soc.* **113**, 7433 (1991).
- G. D. Van Duyn, R. F. Standaert, P. A. Karplus, S. L. Schreiber, J. Clardy, *J. Mol. Biol.* **229**, 105 (1993).
- C. R. Kissinger *et al.*, *Nature* **378**, 541 (1995).
- J. P. Griffith *et al.*, *Cell* **82**, 507 (1995).
- J. Chen, X. F. Zheng, E. J. Brown, S. L. Schreiber,

Proc. Natl. Acad. Sci. U.S.A. 92, 4947 (1995).

23. The expression and purification of recombinant human FKBP12 (19) and the FRB domain of human FRAP (22) have been described. Crystals of FKBP12-rapamycin-FRB were grown in 2 to 3 weeks at room temperature from hanging drops prepared from FKBP12 [10 mg/ml, in 10 mM tris-HCl (pH 8.0)], two equivalents of rapamycin (in methanol), and one equivalent of FRB [10 mg/ml, in 50 mM tris-HCl (pH 8.0)]. The well solution contained 20% (w/v) polyethylene glycol 8000, 10% methypentandiol, and 10 mM tris-HCl (pH 8.5). The rod-shaped crystals are orthorhombic, space group $P2_12_12_1$, with cell constants $a = 44.63$, $b = 52.14$, and $c = 102.53$ Å, and contain one ternary complex in the asymmetrical unit.
24. Data to a resolution of 2.7 Å (43,447 measurements of 6920 unique reflections, 98.5% complete, $R_{\text{sym}} = 0.071$) were collected from a crystal of dimensions 0.3 mm by 0.2 mm by 0.1 mm with the use of a San Diego multiwire area detector on a Rigaku RU-200 rotating anode x-ray source. Experimental phases were obtained from MR and SIRAS. MR with X-PLOR [A. T. Brünger, J. Kuriyan, M. Karplus, *Science* 235, 458 (1987)] and the FKBP12-rapamycin model (19) yielded a clear solution, but the resulting electron density map was noisy. A mercury derivative was prepared (2 mM HgCl_2 , overnight), and the two heavy atom sites were refined with PHASES [W. Furey and S. Swaminathan, *ACA Abstr.* 18, 73 (1990)]. Anomalous dispersion measurements were included in this data set and 16 cycles of solvent flattening were applied (PHASES). The resulting electron density map clearly showed the four-helix-bundle architecture of FRB. The FKBP12-rapamycin portion of the structure was well defined in the initial electron density map, and minor changes in the backbone of the 30s loop and some side chains were sufficient to fit the model. For the FRB portion, most of a polyalanine chain could be traced for the helical regions of the initial map. After several cycles of positional refinement (X-PLOR), loop regions could also be traced and the side chains assigned. CHAIN [J. S. Sack, *J. Mol. Graphics* 6, 244 (1988)] was used for model fitting and building the structure. A total of 95 residues in the FRB domain of FRAP (three residues in the NH_2 -terminal and two residues in the COOH -terminal regions showed no electron density and were not included), all residues of FKBP12, all atoms of rapamycin, and 23 water molecules were included in the final model. FRB residues are numbered according to FRAP numbering. The current R factor is 0.193 ($R_{\text{free}} = 0.299$) for data from 8 to 2.7 Å. The root-mean-square deviations of bond lengths and bond angles are 0.008 Å and 1.48° , respectively. The average temperature factors for all atoms and main chain atoms are 17.0 and 14.7 Å², respectively.
25. N. L. Harris, S. R. Presnell, F. E. Cohen, *J. Mol. Biol.* 236, 1356 (1994).
26. F. Lederer, A. Glatigny, P. H. Bethge, H. D. Bellamy, F. S. Mathews, *ibid.* 148, 427 (1981).
27. J. A. Findlay and L. Radics, *Can. J. Chem.* 58, 579 (1980).
28. X. F. Zheng, D. Fiorentino, J. Chen, G. R. Crabtree, S. L. Schreiber, *Cell* 82, 121 (1995).
29. M. C. Lorenz and J. Heitman, *J. Biol. Chem.* 270, 27531 (1995).
30. V. M. Rivera et al., *Nature Med.*, in press.
31. M. Carson, *J. Mol. Graphics* 5, 103 (1987).
32. A. C. Wallace, R. A. Laskowski, J. M. Thornton, *Prot. Engin.* 8, 127 (1995).
33. A. Nicholls, K. Sharp, B. Honig, *GRASP Manual* (Columbia Univ. Press, New York, 1992).
34. We thank S. Ealick, J. Liang, and R. Gillilan for discussions. The Cornell work was funded in part by USPHS grant CA59021 (to J.C.) and the Harvard work by an Irvington Institute Fellowship (to J.C.) and USPHS grant GM38625 (to S.L.S.). S.L.S. is a Howard Hughes Medical Institute Investigator. Atomic coordinates have been deposited in the Protein Data Bank under the accession number 1FAP.

15 March 1996; accepted 15 May 1996

Long-Term Lymphohematopoietic Reconstitution by a Single CD34-Low/Negative Hematopoietic Stem Cell

Masatake Osawa,* Ken-ichi Hanada, Hirofumi Hamada, Hiromitsu Nakauchi†

Hematopoietic stem cells (HSCs) supply all blood cells throughout life by making use of their self-renewal and multilineage differentiation capabilities. A monoclonal antibody raised to the mouse homolog of CD34 (mCD34) was used to purify mouse HSCs to near homogeneity. Unlike in humans, primitive adult mouse bone marrow HSCs were detected in the mCD34 low to negative fraction. Injection of a single mCD34^{low/-}, c-Kit⁺, Sca-1⁺, lineage markers negative (Lin⁻) cell resulted in long-term reconstitution of the lymphohematopoietic system in 21 percent of recipients. Thus, the purified HSC population should enable analysis of the self-renewal and multilineage differentiation of individual HSCs.

CD34 is a marker of human HSCs, and all colony-forming activity of human bone marrow (BM) cells is found in the CD34-positive fraction (1). Clinical transplantation studies that used enriched CD34⁺ BM cells also indicated the presence of HSCs with long-term BM reconstitution ability within this fraction (2). After isolation of the human CD34 gene, the mouse homolog (mCD34) was isolated by cross-hybridization (3). To examine the expression and function of mCD34, we raised a monoclonal antibody (mAb), 49E8 [rat immunoglobulin G2a (IgG2a)], to mCD34 by immunizing rats with a glutathione-S-transferase (GST)-mCD34 fusion protein. This mAb stained BaF3 cells transfected with a full-length mCD34 cDNA but not mock-transfected cells (4). Murine cell lines such as PA6, NIH 3T3, M1, and DA1, shown by reverse transcriptase-polymerase chain reaction (RT-PCR) to contain mCD34 mRNA, were also stained by this mAb, indicating that 49E8, although specific for a GST-mCD34 fusion protein, could also recognize the native form of mCD34 as expressed on various cell types (4).

We next examined adult mouse BM for expression of mCD34. Four-color fluorescence-activated cell sorter (FACS) analysis was done after sequential staining of BM cells with a combination of lineage-specific mAbs to CD4, CD8, B220, Gr-1, Mac-1, and TER119, and then a mixture of mAbs to c-Kit (ACK-2), Ly6A/E (Sca-1), and mCD34 (5).

M. Osawa and H. Nakauchi, Department of Immunology, Institute of Basic Medical Sciences and Center for Tsukuba Advanced Research Alliance, University of Tsukuba, Tsukuba Science-City, Ibaraki 305, Japan. K.-i. Hanada and H. Hamada, Department of Molecular Biotherapy, Cancer Chemotherapy Center, Japanese Foundation for Cancer Research, Tokyo 170, Japan.

*Present address: KIRIN Pharmaceutical Research Laboratory, Gunma 371, Japan.

†To whom correspondence should be addressed.

Monoclonal antibody 49E8 reacted with $2.5 \pm 0.5\%$ (mean \pm SD) of total BM cells, with most of the positive cells occurring in the Lin⁻ fraction (Fig. 1A). More than 90% of the c-Kit⁺ Sca-1⁺ Lin⁻ cells previously shown to contain primitive HSCs (6) stained brightly with 49E8, whereas the remainder were low to negative (Fig. 1B). The frequency of mCD34⁺ c-Kit⁺ Sca-1⁺ Lin⁻ cells and mCD34⁻ c-Kit⁺ Sca-1⁺ Lin⁻ cells among total nucleated BM cells was $0.073 \pm 0.028\%$ (mean \pm SD, $n = 5$) and $0.004 \pm 0.003\%$ (mean \pm SD, $n = 5$), respectively.

To determine whether mouse HSCs express mCD34, we sorted subpopulations by FACS and examined their stem cell activity. Within the c-Kit⁺ Sca-1⁺ Lin⁻ population, the frequency of interleukin-3 (IL-3)-dependent colony-forming unit culture (CFU-C) per 200 cells was $20.0 \pm 3.9\%$ (mean \pm SD, $n = 8$) (7) for mCD34⁺ cells but only $0.16 \pm 0.4\%$ (mean \pm SD, $n = 8$) in the CD34⁻ fraction. Similarly, mCD34⁺ cells contained $14.1 \pm 3.4\%$ (mean \pm SD, $n = 15$) day 12 CFU spleen (CFU-S) per 200 cells, whereas in the mCD34⁻ fraction this value was $1.6 \pm 1.7\%$ (mean \pm SD, $n = 15$) (8). Thus, colony-forming activity was positively correlated with mCD34 expression among c-Kit⁺ Sca-1⁺ Lin⁻ cells. When these cells were cultured in the presence of both IL-3 and stem cell factor (SCF), however, 80% of mCD34⁻ c-Kit⁺ Sca-1⁺ Lin⁻ cells formed large multilineage colonies (7).

For in vivo analyses, c-Kit⁺ Sca-1⁺ Lin⁻ cells were fractionated into mCD34^{low/-} (Fr. 1), mCD34^{hi} (Fr. 2), and CD34⁺ (Fr. 3) subpopulations according to their mCD34 expression by FACS (Fig. 2A). Although 100 c-Kit⁺ Sca-1⁺ Lin⁻ cells were sufficient to radioprotect a lethally irradiated mouse, injection of 300 cells from either the Fr. 1 or Fr. 3 subpopulation (Fig. 2A) alone showed poor radioprotective ability (9). When cells

REPORTS

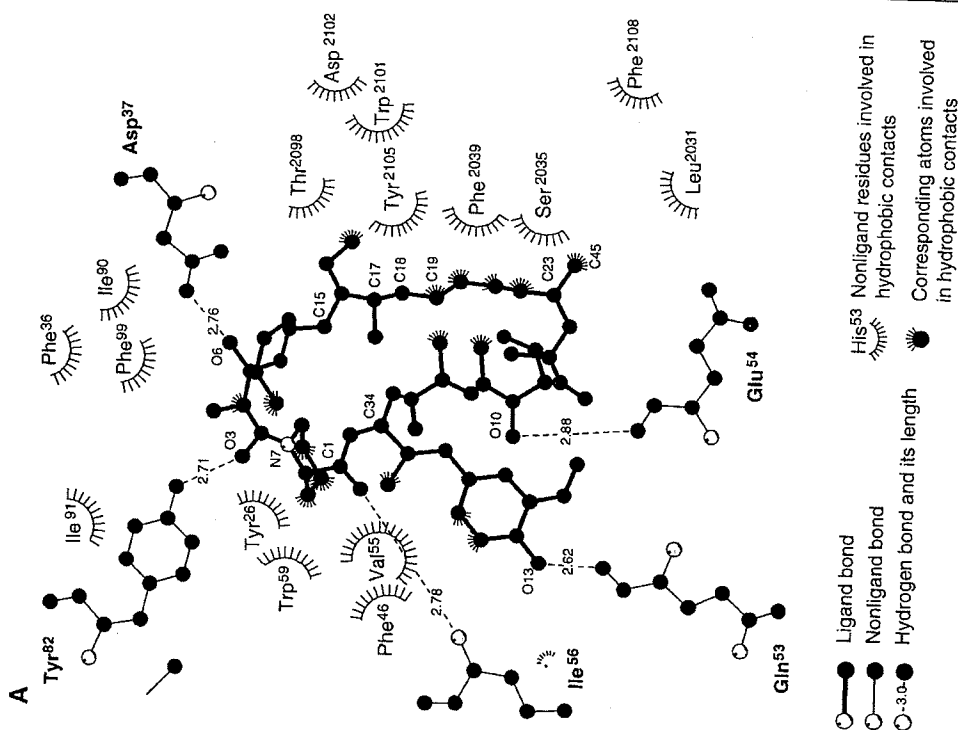
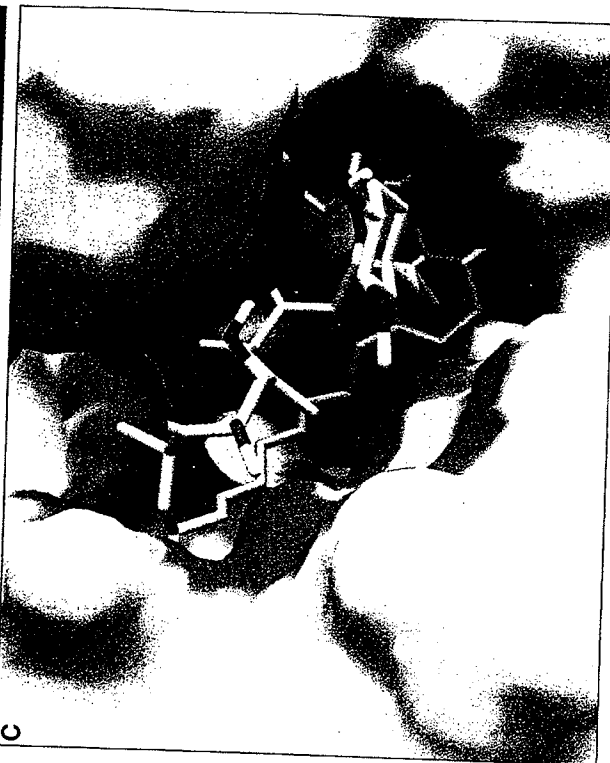
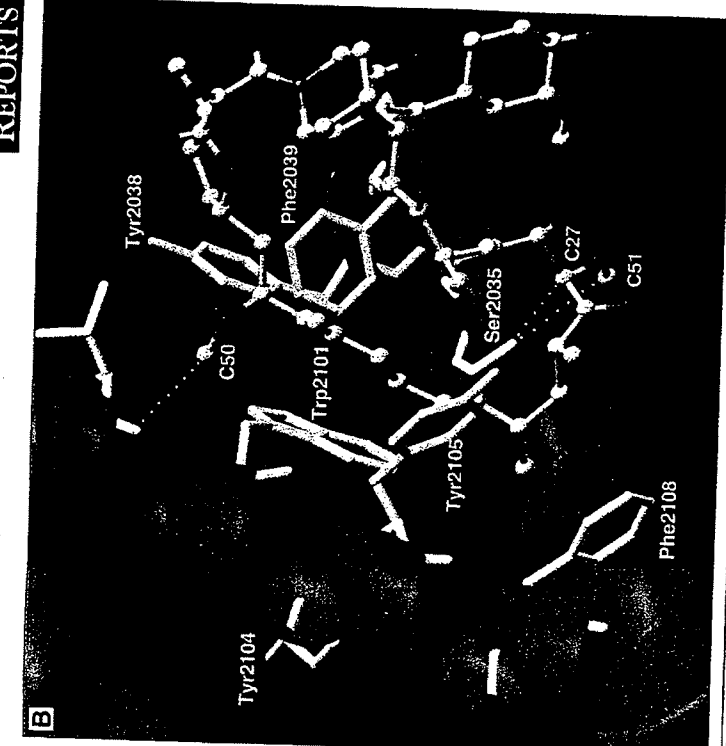


Fig. 2. Interactions of rapamycin with FKBP12 and FRB. **(A)** A LIGPLOT (32) rendering of the interactions of rapamycin with FKBP12 and FRB. Hydrogen bonds are shown by dashed lines (with lengths in angstroms), and hydrophobic interactions by surface dashes. **(B)** Close-up of the interactions of rapamycin (ball and stick) with the FRB domain of FRAP (red ribbon). Residue numbering is based on that for FRAP. **(C)** Complementarity plot of rapamycin with FKBP12 and the FRB domain of FRAP (33). High complementarity is indicated by purple. FKBP12 is on the right and the opening of the deep cavity where the piperidyl moiety is buried is visible. The FRB domain of FRAP is on the left, and the most deeply buried methyl group is shown disappearing into the FRB cavity.

FRAP) so that the FRB pocket is optimized for rapamycin binding.

protein interactions, rapamycin-induced dimerization does not. Because rapamycin-

8. H. Tanaka et al., *J. Am. Chem. Soc.* 109, 5031 (1987).

rapamycin—and thus all four domains—contain a hydrophobic architecture and related interactions of the Ser1972 (corresponding to the Ser1972 in FKBP12).

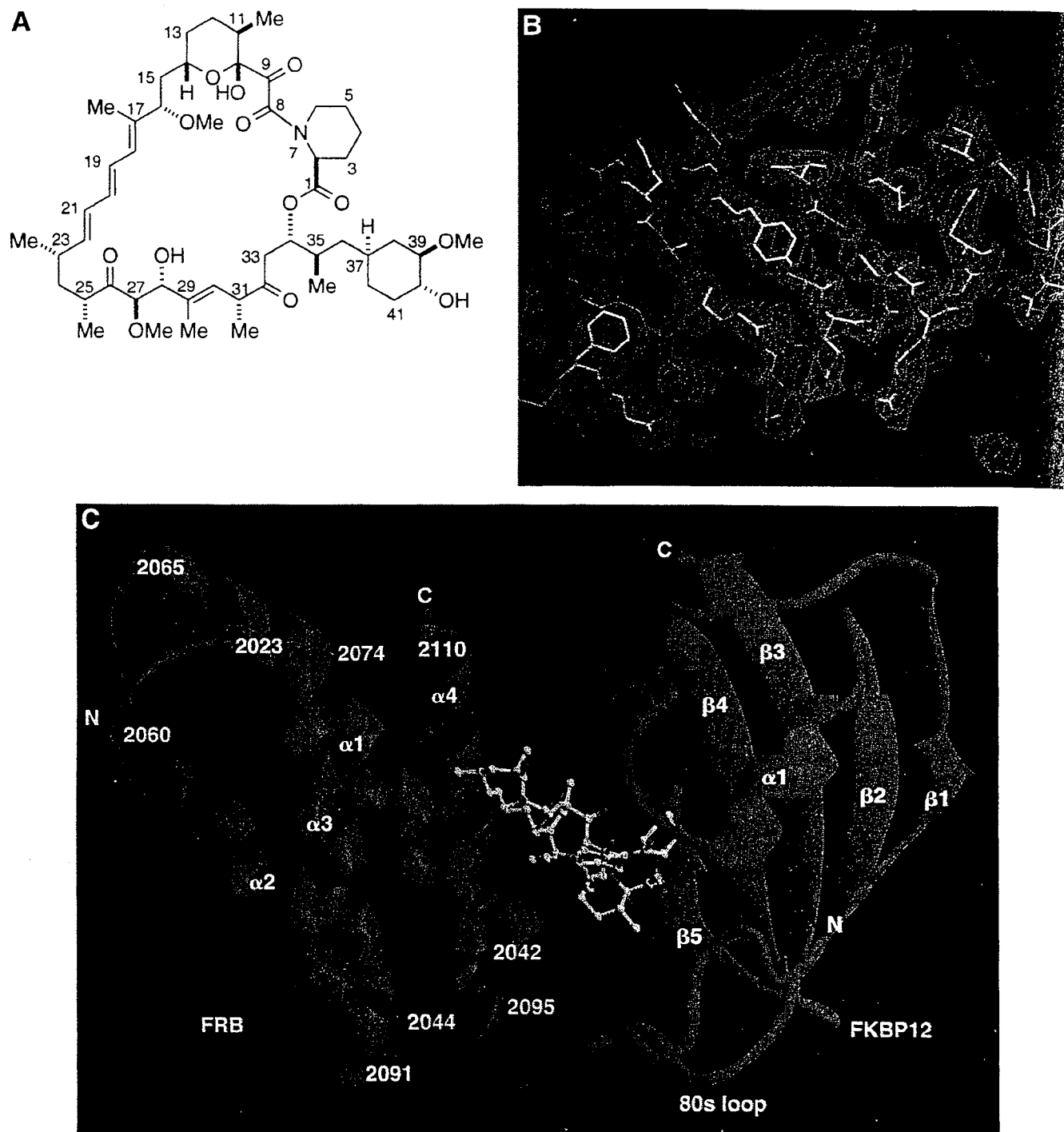


Fig. 1. (A) Chemical structure of rapamycin. **(B)** The $2F_o - F_c$ electron density of the FRB domain of the FKBP12-rapamycin-FRB complex (24) (F_o , observed structure factor; F_c , calculated structure factor). A model of the final structure is embedded in this initial electron density. **(C)** Overall structure of the ternary complex between FKBP12 (blue ribbon), rapamycin (ball and stick), and the FRB domain of FRAP (red ribbon). Secondary structural elements are labeled with the conventional numbering scheme for FKBP12. N and C, NH_2 - and COOH -termini, respectively. The drawing in (C) was prepared with RIBBONS (31).

action region, the NH_2 group of Arg²⁰⁴² makes short contacts with $\text{O}\gamma 1$ of Thr⁸⁵ and the O atom of Gly⁸⁶, and there are two water-

bind FKBP12-rapamycin—and thus all four proteins are likely to contain a hydrophobic pocket with similar architecture and related



Automated, fast and sensitive quantification of drugs in blood by liquid chromatography–mass spectrometry with on-line extraction: immunosuppressants

Uwe Christians^{a,b,*}, Wolfgang Jacobsen^a, Natalie Serkova^a, Leslie Z. Benet^a, Christian Vidal^b, Karl-Fr. Sewing^b, Michael P. Manns^c, Gabriele I. Kirchner^c

^aDepartment of Biopharmaceutical Sciences, University of California, San Francisco, CA 94143-0446, USA

^bInstitut für Pharmakologie, Medizinische Hochschule Hannover, 30623 Hannover, Germany

^cAbteilung Gastroenterologie und Hepatologie, Medizinische Hochschule Hannover, 30623 Hannover, Germany

Received 2 March 2000; received in revised form 18 June 2000; accepted 28 June 2000

Abstract

We developed a universal LC–mass spectrometry assay with automated online extraction (LC/LC–MS) to quantify the immunosuppressants cyclosporine, tacrolimus, sirolimus and SDZ-RAD alone or in combination in whole blood. After protein precipitation, samples were loaded on a C₁₈ extraction column, were washed and, after activation of the column-switching valve, were backflushed onto the C₈ analytical column. [M• Na]⁺ ions were detected in the selected ion mode. For tacrolimus, sirolimus and SDZ-RAD, the assay was linear from 0.25 to 100 • g/l and for cyclosporine from 7.5 to 1250 • g/l (all r^2 • 0.99). Analytical recovery was • 85% and, in general, inter-day, intra-day variability for precision and accuracy were • 10%. © 2000 Elsevier Science B.V. All rights reserved.

Keywords: Sample preparation; Cyclosporine; Tacrolimus; Sirolimus; SDZ-RAD

1. Introduction

Today, the calcineurin inhibitors cyclosporine and tacrolimus are the basis of most immunosuppressive protocols after organ transplantation. In addition, they are used in the therapy of autoimmune diseases [1–3]. Sirolimus and SDZ-RAD have immunosuppressive mechanisms distinct from those of cyclosporine and tacrolimus. Sirolimus and SDZ-RAD inhibit interleukin-2-stimulated cell cycle progression

at the G₁–S interface [4–6]. Co-administration of cyclosporine with sirolimus or SDZ-RAD results in synergistic immunosuppression [6–9] and significantly less rejection of transplant organs [10,11]. The combination of tacrolimus and sirolimus is also beneficial for transplant patients [12,13]. Sirolimus has recently been approved in the US [14] and SDZ-RAD is in phase III of its clinical development.

Cyclosporine is a cyclic undecapeptide (molecular mass, 1203.6 Da). Tacrolimus, sirolimus and SDZ-RAD have macrolide backbone structures (Fig. 1). Tacrolimus (molecular mass, 803.5 Da) is a macrolide lactone with a hemi-ketal masked •,•-diketoamide functionality in a 23-membered ring.

*Corresponding author. Tel.: • 1-415-502-4968; fax: • 1-415-502-8139.

E-mail address: uwec@itsa.ucsf.edu (U. Christians).

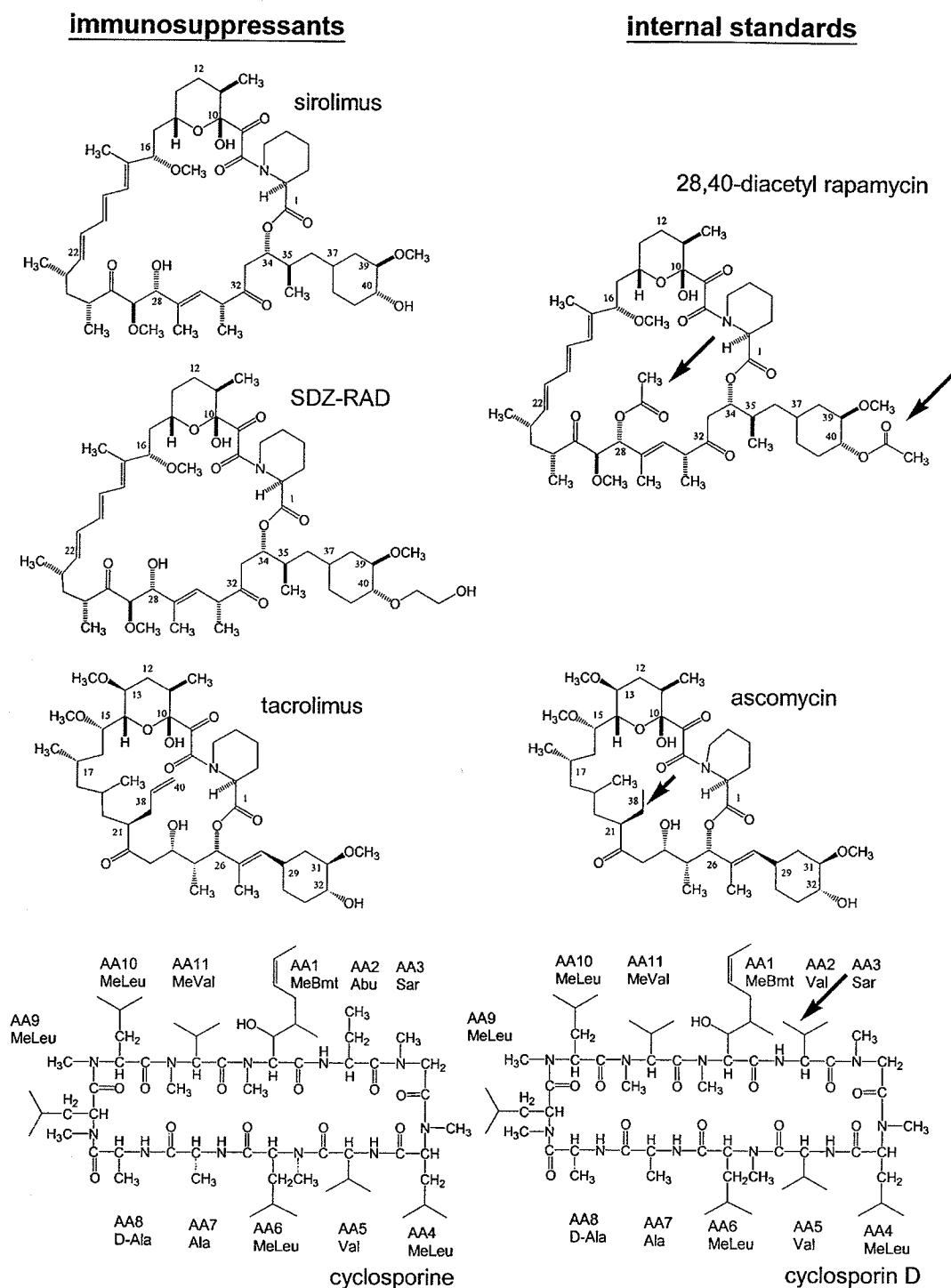


Fig. 1. Structures of the immunosuppressants and their internal standards. Numbering of the macrolide immunosuppressants sirolimus, SDZ-RAD, and tacrolimus and their internal standards follows the IUPAC guidelines [30]. The arrows indicate the structural differences between the internal standards and the corresponding immunosuppressant(s). AA, amino acid.

Sirolimus (rapamycin, molecular mass, 913.6 Da) is a 31-membered triene macrolide lactone with a hemiketal-masked α,β -dioxocarboxamide. SDZ-RAD (molecular mass, 957.2 Da) is the semi-synthetic 40-*O*-(2-hydroxyethyl) derivative of rapamycin [15]. The study drugs have in common that they are soluble in alcohols, acetonitrile, ethers and halogenated hydrocarbons and they are practically insoluble in water and aliphatic hydrocarbons.

The clinical management of cyclosporine and tacrolimus is complicated by their narrow therapeutic indices, intra- and inter-individually highly variable pharmacokinetics, and the lack of a reliable correlation between dose and drug exposure. The four immunosuppressants are mainly metabolized by cytochrome P4503A in the liver and small intestine [16–18] and are substrates of the ATP-binding cassette transporter P-glycoprotein [19]. Several drugs commonly used after transplantation, which are cytochrome P4503A and/or P-glycoprotein substrates, inhibitors and/or inducers, affect blood concentrations of immunosuppressants with the requirement for dose adjustments [20]. Therefore, regular therapeutic drug monitoring and blood concentration guided dosing regimens have been recommended [21–25]. These are general clinical practice for cyclosporine and tacrolimus [21–24] and are discussed for sirolimus [25,26] and SDZ-RAD [11]. For therapeutic drug monitoring of cyclosporine, tacrolimus, sirolimus and SDZ-RAD, several assays are available [23,24]. In clinical routine monitoring immunoassays are mostly used. However, these have the disadvantage that the antibodies used cross-react to a varying extent with metabolites, the immunosuppressants cannot be measured simultaneously and immunoassays are either not available or approved for all immunosuppressants, for example sirolimus [23] and SDZ-RAD.

Increasingly, immunosuppressive drug regimens used after transplantation are based on a combination of two and more immunosuppressants, which require blood level-guided dosing [23,24]. In the near future, more novel immunosuppressive drugs will become available and immunosuppressive drug regimens will be even more individualized. Analytical laboratories will consequently be challenged with blood samples containing a variety of different immunosuppressants and their combinations with relatively few samples

containing the same drugs [24]. It was therefore our goal, to develop a single analytical assay for the automated, specific and sensitive measurement of immunosuppressants alone and in combination. Based on our previous work [27–29], we used LC–MS in combination with a rapid automated online extraction procedure (LC/LC–MS).

2. Experimental

2.1. Chemicals

Cyclosporine, SDZ-RAD (40-(2-hydroxyethyl)-rapamycin) and cyclosporin D were kind gifts of Novartis Pharma (Basel, Switzerland) and tacrolimus the kind gift of Fujisawa Healthcare (Deerfield, IL, USA). Sirolimus (rapamycin) and ascomycin were purchased from Sigma (St. Louis, MO, USA). 28,40-*O*-Diacetyl rapamycin was synthesized, purified, the structure verified and purity established as described by Streit et al. [31]. Methanol and water were of HPLC grade and purchased from Fisher Scientific (Fair Lawn, NJ, USA). Formic acid and zinc sulfate were from Sigma, and were of reagent grade.

2.2. Equipment

Samples were analyzed on a Hewlett-Packard (Palo Alto, CA, USA) LC/LC–mass selective detector system consisting of the following series 1100 HPLC components. HPLC I: G1311A quaternary pump, G1322A degasser and G1329A autosampler equipped with a G1330A thermostat. HPLC II: G1312A binary pump, G1322A degasser, G1316A column thermostat and G1946A mass selective detector. The two HPLC systems were connected via a 7240 Rheodyne six-port switching valve mounted on a step motor (Rheodyne, Cotati, CA) (see Fig. 2). The system was controlled and data were processed using ChemStation Software Revision A.06.01 (Hewlett-Packard).

2.3. Stock solutions

Stock solutions were prepared from three independent weighings. The immunosuppressants (cyclosporine, tacrolimus, sirolimus and SDZ-RAD) and the

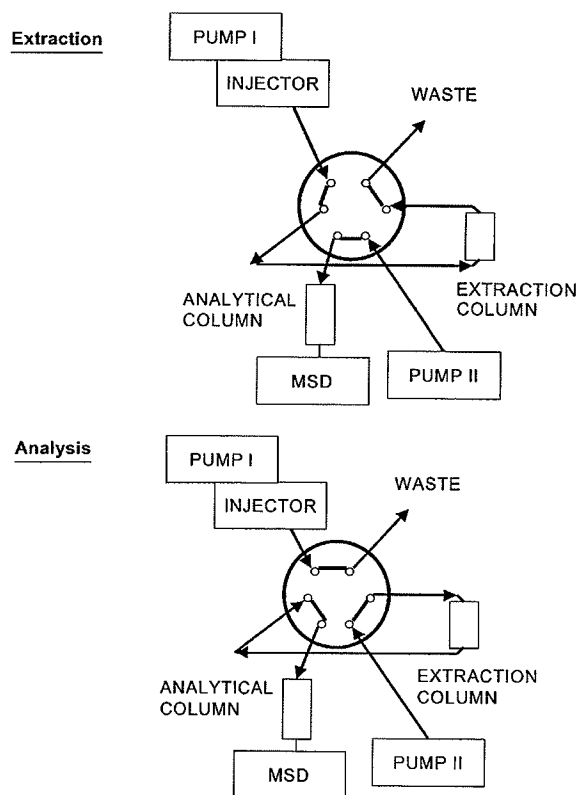


Fig. 2. Connection of the column switching valve and valve positions. HPLC 1, pump I, injector, extraction column; HPLC 2, pump II, analytical column, mass selective detector. MSD, mass selective detector.

internal standards (cyclosporin D, ascomycin and 28,40-*O*-diacetyl rapamycin; structures see Fig. 1) were dissolved in methanol–0.1% formic acid (9/1, v/v), resulting in a concentration of 1 g/l. For the final preparation of calibration and quality control samples as well as internal standard solutions, stock solutions were diluted using methanol–0.1% formic acid. Due to the instability of sirolimus, SDZ-RAD and 28,40-*O*-diacetyl rapamycin, stock solutions had to be stored at -80°C [31,32].

2.4. Blood samples

Blood for development and validation of the assay was drawn from healthy volunteers. EDTA was used as anticoagulant. Patient samples were drawn during various clinical studies. Collection of blood samples and quantification of immunosuppressants were part

of the study protocols. The studies were approved by either the Stanford University or the University of California, San Francisco, ethics committees. All subjects gave their written consents and the studies were carried out in compliance with the Declaration of Helsinki and its amendments following good clinical practice (GCP) guidelines. Blood samples were stored at -80°C .

2.5. Sample preparation (see Table 1)

As a first step, the internal standards were added to the protein precipitation reagent (methanol–0.4 M ZnSO_4 , 4/1, v/v) resulting in final concentrations of 250 $\mu\text{g/l}$ cyclosporin D and 50 $\mu\text{g/l}$ ascomycin and 28,40-*O*-diacetyl rapamycin. Due to the instability of 28,40-*O*-diacetyl rapamycin [31,32], the protein precipitation/internal standard solution had to be freshly prepared before extraction. The internal standard concentrations correspond to addition of 500 μg

Table 1
Comparison of sample preparation steps of blood samples for LC/LC-MS and LC-MS analysis^a

LC/LC-MS	LC-MS
0.1 ml blood + internal standard + 0.2 ml 0.2 mol/l ZnSO_4 / methanol (30/70 v/v)	1 ml blood + internal standard + 2 ml 0.2 mol/l ZnSO_4 / methanol (30/70 v/v)
↓	↓
vortex 20 s	vortex 20 s
centrifugation 8000 $\times g$, 5 min	centrifugation (2000 $\times g$, 2 min)
↓	↓
	Column preparation: + 2 ml methanol + 2 ml 0.1% formic acid
	draw supernatant through column (–15 mmHg vacuum)
	+ 2 ml 0.1% formic acid
	↓
	dry column
	elution with 1.5 ml dichloromethane
	↓
	evaporate to dryness
	↓
	reconstitute in 120 μl methanol / 0.1% formic acid
	↓
inject 100 μl into LC/LC-MS	inject 100 μl into LC-MS system

^a The LC-MS sample preparation procedure was used for SDZ-RAD [32], and with small modifications for tacrolimus [33,34] and sirolimus [31].

cyclosporin D and 100 • g ascomycin and 28,40-diacetyl rapamycin to a 1-ml blood sample.

One hundred • l of the blood sample were transferred into an Eppendorf cup and 200 • l of the protein precipitation reagent were added (Table 1). Samples were vortexed for 20 s and centrifuged at 8000 g for 5 min. Two-hundred • l of the supernatant were transferred into HPLC screw cap vials with 250-• l inserts (Hewlett-Packard).

2.6. LC/LC–MS analysis (Table 2)

One hundred • l of the samples were injected onto a 10• 2-mm extraction column (Keystone Scientific, Bellefonte, PA) filled with Hypersil ODS-1 of 10 • m particle size (Shandon, Chadwick, UK). Samples were washed with a mobile phase of 40% methanol and 60% 0.1% formic acid supplemented with 1 • mol/l sodium formate. The flow was 5 ml/min and the temperature for the extraction column was set to 65•C. After 0.75 min, the switching valve was activated (Fig. 2) and the analytes were eluted in the backflush mode from the extraction column onto the 50• 4.6-mm C₈, 3.5 • m analytical column (Zorbax

XDB C₈, Hewlett-Packard, Palo Alto, CA). The mobile phase consisted of methanol and 0.1% formic acid supplemented with 1 • mol/l sodium formate. The following gradient was run (Table 2): time 0 min, 65% methanol; 9 min, 95% methanol. The flow-rate was 0.4 ml/min. The analytical column was also kept at 65•C. Two minutes after sample injection, the mass-selective detector was activated. Settings of the mass selective detector are listed in Table 3. The next sample was injected after 9.5 min.

2.7. Method validation

2.7.1. Calibration and calibration control samples

Precision control samples (concentrations see Table 4) and calibration control samples (cyclosporine: 5, 7.5, 10, 25, 50, 100, 250, 500, 750, 1000, 1250, 1500 • g/l; tacrolimus, sirolimus, SDZ-RAD: 0.1, 0.25, 0.5, 1, 5, 1, 20, 50, 75 and 100 • g/l) as well as blank samples were prepared in bulk using freshly drawn blood. To allow distribution, samples were incubated at 37•C in a water bath for 30 min. Then 1-ml aliquots were transferred into screw-cap glass tubes and either immediately analyzed or stored at • 80•C.

2.7.2. Acceptance criteria

The assay was considered acceptable if precision (% C.V.) at each concentration was less than 15% for intra- and day-to-day variability. The accuracy compared with the nominal value had to be within • 15% for both intra- and day-to-day variability. The calibration curve had to have a correlation coefficient r^2 of 0.99 or better. The absolute recovery had to exceed 60%.

2.7.3. Calibration curve

Six samples of each concentration were measured. Linearity was assessed using the regression analysis implemented in the Microcal Origin software (version 3.5, Microcal Software, Northampton, MA, USA).

2.7.4. Lower limit of quantitation.

The lowest concentration that met the following criteria was accepted as the lower limit of quantitation: 80% of the samples analyzed had to be within • 20% of the nominal value, and precision and accuracy variation had to be less than 20%.

Table 2
Time programs for solvent delivery pumps (HPLC I and HPLC II), column switching valve and mass selective detector (MSD)^a

Time	HPLC I	HPLC II	Column switch
0.00 min	40% methanol 5 ml/min	65% methanol 0.4 ml/min	Valve in extraction position
0.70 min	40% methanol 5 ml/min		Valve switches to analysis position
0.80 min	95% methanol 0.1 ml/min		2.00 min MSD on
6.80 min	95% methanol 0.1 ml/min		Valve switches back to extraction position
6.81 min	95 % methanol 5 ml/min		
8.00 min	40% methanol 5 ml/min	95% methanol 0.4 ml/min	
9.00 min		95% methanol 0.4 ml/min	9.00 min: MSD off
9.50 min		65% methanol 0.4 ml/min	

^a Columns for the solvent delivery pumps (HPLC I and HPLC II) show the solvent composition (percent organic solvent, other solvent: 0.1% formic acid• 1 • mol/l sodium acetate) and the flow-rate.

Table 3
Mass selective detector settings^a

Parameter	
Capillary exit voltage (fragmentor)	• 160 V
Capillary voltage (V_{cap})	• 4000 V
Ion energy (octopole)	• 5 V
Nebulizer gas	Nitrogen, purity 5.0; pressure, 40 p.s.i. (1 p.s.i. • 6.894.76 Pa)
Drying gas	Nitrogen, purity 5.0; temperature, 300°C; flow, 10 l/min
Quadrupole temperature	100°C
Selected ions	<i>m/z</i>
Cyclosporine	1224: cyclosporine, 1238: cyclosporin D (internal standard)
Tacrolimus	826: tacrolimus, 815: ascomycin (internal standard)
Rapamycin, SDZ-RAD	936: sirolimus, 980: SDZ-RAD, 1020: 28,40-diacetyl rapamycin (internal standard)
Dwell time/ion	124 ms

^a Positive ions $[M + Na]^+$ were measured in the selected ion mode. The nomenclature follows that used in the ChemStation software (revision A.06.01, Hewlett-Packard).

2.7.5. Day-to-day and intra-day precision, accuracy

Intra-day precision and accuracy were evaluated from the results of the quality control samples

processed the same day ($n = 10$ for each concentration). Day-to-day variability was assessed by analysis of five sets of quality control samples on three different days.

Table 4
Validation results

	Cyclosporine		SDZ-RAD		Sirolimus		Tacrolimus	
Lower limit of quantitation	7.5 • g/l		0.25 • g/l		0.25 • g/l		0.25 • g/l	
Upper limit of quantitation	1250 • g/l		100 • g/l		100 • g/l		100 • g/l	
Regression analysis	$y = 0.93(\pm 0.03) \cdot x$		$y = 0.96(\pm 0.03) \cdot x$		$y = 0.99(\pm 0.02) \cdot x$		$y = 0.94(\pm 0.01) \cdot x$	
	15.1(17.4)		0.05(• 0.04)		0.09(• 0.08)		0.06(• 0.06)	
	$r^2 = 0.995$		$r^2 = 0.999$		$r^2 = 0.990$		$r^2 = 0.999$	
Intra-day precision	7.5 • g/l:	2.5%	1 • g/l:	2.5%	1.5 • g/l:	7.2%	0.25 • g/l:	12.3%
	125 • g/l:	3.9%	5 • g/l:	3.9%	15 • g/l:	5.5%	1 • g/l:	3.7%
	375 • g/l:	0.9%	25 • g/l:	0.9%	40 • g/l:	6.2%	25 • g/l:	1.5%
	1250 • g/l:	2.6%	100 • g/l:	2.6%			100 • g/l:	15.8%
Day-to-day precision	75 • g/l:	2.5%	1 • g/l:	6.5%	1.5 • g/l:	7.1%	5 • g/l:	4.4%
	200 • g/l:	3.6%	25 • g/l:	5.5%	15 • g/l:	9.8%	20 • g/l:	0.7%
	700 • g/l:	2.7%	100 • g/l:	9.1%	40 • g/l:	6.7%	70 • g/l:	1.6%
Accuracy	75 • g/l:	• 0.9%	1 • g/l:	• 7.1%	1.5 • g/l:	• 3.7%	5 • g/l:	• 3.4%
	200 • g/l:	• 4.1%	25 • g/l:	• 2.6%	15 • g/l:	• 7.4%	20 • g/l:	• 8.6%
	700 • g/l:	• 2.6%	100 • g/l:	• 3.8%	40 • g/l:	• 8.0%	70 • g/l:	• 3.6%

2.7.6. Recovery

Recoveries were calculated from the quality control samples ($n = 6$ for each concentration). The mass spectrometer responses of the extracted samples were compared with the response after injection of respective amounts of internal standard or standard solutions of the immunosuppressants (in methanol–0.1% formic acid, 9:1, v/v) directly on the analytical column, bypassing the extraction column.

2.7.7. Matrix interferences and carry-over effects

The lack of matrix interferences was established by analysis of blank blood samples ($n = 6$). The lack of carry-over effects was assessed by alternately analyzing blank blood samples ($n = 6$) and blood samples containing concentrations of the immunosuppressants at the upper limit of quantitation ($100 \text{ } \mu\text{g/l}$, $n = 6$).

2.7.8. Within-batch stability

Stability of the immunosuppressants and their internal standards after protein precipitation in the autosampler was established for 48 h. Ten sets of quality control samples were prepared as described in Section 2.5, and placed into the autosampler adjusted to 10°C . Five sets were analyzed at once (controls) and five sets 48 h later.

3. Results

The recoveries of the study drugs after protein precipitation and column switching were: cyclosporine, $91.3 \pm 9.8\%$; tacrolimus, $96.2 \pm 5.6\%$; sirolimus, $88.0 \pm 12.1\%$; and SDZ-RAD, $86.1 \pm 9.9\%$ (means \pm standard deviation). The recoveries of the internal standards were not significantly different from those of the immunosuppressants. Comparison of peak areas after injection of immunosuppressant solutions ($10 \text{ } \mu\text{l}$ of 1 mg/l in methanol–0.1% formic acid, $n = 5$) into the LC/LC–MS system with those after injection of the same solution directly onto the analytical column showed that no drug was lost during the online extraction procedure (cyclosporine, $101 \pm 3.2\%$; tacrolimus, $99.6 \pm 5.5\%$; sirolimus, $102.3 \pm 3.4\%$; SDZ-RAD, $98.8 \pm 5.0\%$) and indicated that losses and most of the variability during extraction had to be attributed to the protein precipitation step.

Under the conditions described, in the positive mode, the immunosuppressants and their internal standards were mainly detected as sodium adducts $[\text{M} + \text{Na}]^+$ (Fig. 3). The intensities of $[\text{M} + \text{H}]^+$ and $[\text{M} + \text{K}]^+$ combined were less than 10% of the $[\text{M} + \text{Na}]^+$ signals.

The lower limit of quantitation of cyclosporine was $7.5 \text{ } \mu\text{g/l}$, and $0.25 \text{ } \mu\text{g/l}$ for the macrolides. Although peaks were detected at lower concentrations with a signal-to-noise ratio above 3, more than 20% (two of six) of the samples were outside the predefined acceptance limits. The upper limit of quantitation was $1250 \text{ } \mu\text{g/l}$ for cyclosporine. Higher concentrations of cyclosporine gave results more than 15% below the nominal concentration in four of six samples. For tacrolimus, sirolimus and SDZ-RAD, the LC/LC–MS assay was linear up to the highest concentration tested ($100 \text{ } \mu\text{g/l}$). Intra-day, day-to-day precision and accuracy were within the pre-defined acceptance limits (Table 4). No matrix interferences or carry-over effects were seen. Within-batch stability was at least 48 h, and thus exceeded the autosampler capacity: It took less than 17 h to run 100 samples with a sample turnover rate of 10 min/sample.

Representative ion chromatograms of patient samples are shown in Figs. 4 and 5.

The methanol–formic acid gradient used to elute the analytes from the analytical column also allowed for separation and simultaneous quantification of the major metabolites of the immunosuppressants. As found for the parent compounds, electrospray ionization of the metabolites yielded $\sim 90\%$ as sodium adducts $[\text{M} + \text{Na}]^+$: cyclosporine: m/z 1256: dihydroxy cyclosporine, m/z 1240: hydroxy cyclosporine (AM1 and AM9 as one peak, AM1c), m/z 1210: AM4N; tacrolimus: m/z 812: 13-*O*-, 15-*O*-, and 31-*O*-desmethyl tacrolimus (Fig. 4C); sirolimus: m/z 952: hydroxy sirolimus, m/z 968: dihydroxy sirolimus, m/z 922: desmethyl sirolimus; SDZ-RAD: m/z 996: hydroxy SDZ-RAD, m/z 966: desmethyl SDZ-RAD. Potential differences of the detector responses of the metabolites and the parent compounds and/or internal standards were assessed by comparison of the peak area ratios (internal standard/metabolite and parent compound/metabolite) after UV and MS detection. The ratios calculated after UV and MS detection were not significantly different from each other (paired *t*-test, $n = 10$ sam-

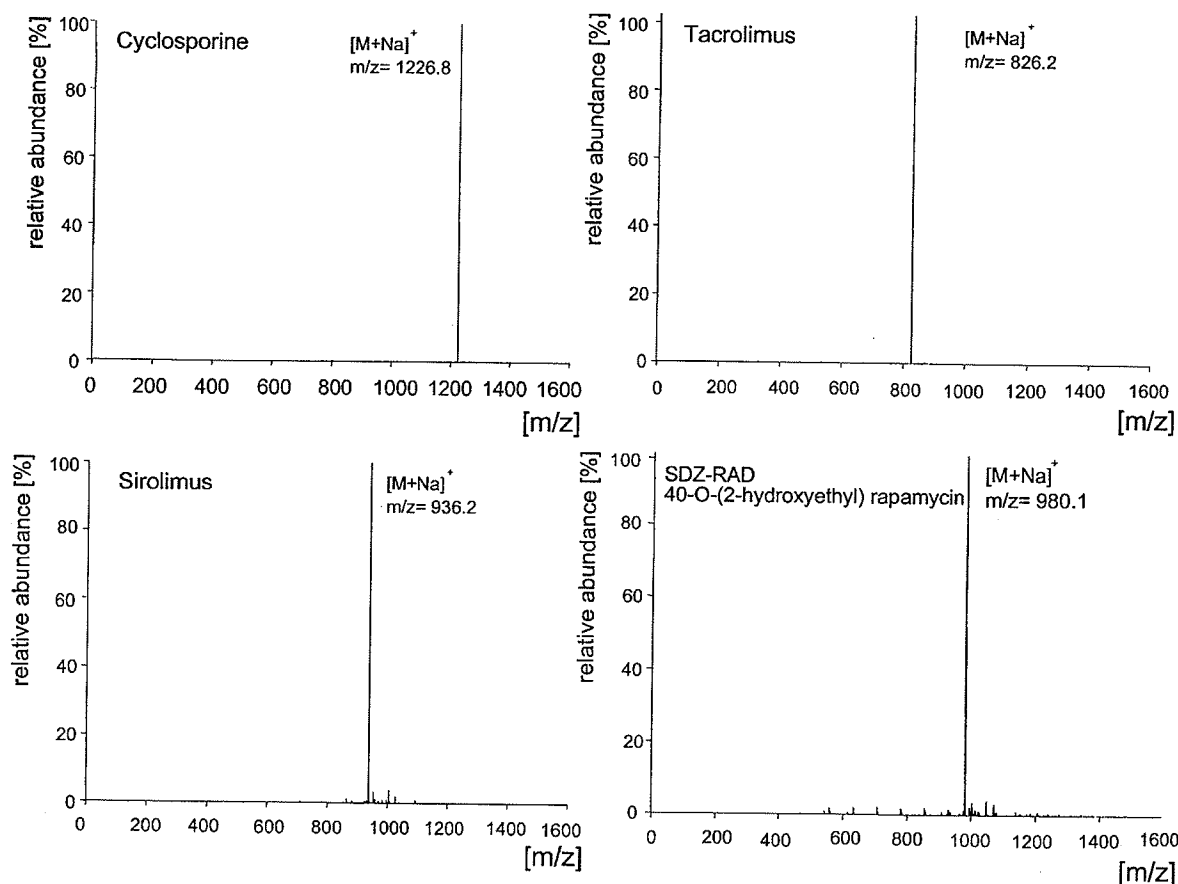


Fig. 3. Full scan mass spectra after injection of the study drugs into the mass spectrometer. Five-hundred ng of the study drugs in 50 μ l methanol–0.1% formic acid (9/1, v/v) were injected into the LC/LC–MS system.

ples), indicating that the internal standards, parent compounds and metabolites resulted in similar detector responses.

As of today, we have used our LC/LC–MS for the measurement of more than 10 000 samples for therapeutic drug monitoring as well as animal and clinical studies. The extraction column was changed every 500 samples. More than 2500 samples were run on an analytical column without loss of sensitivity, accuracy or precision.

4. Discussion

Previously described HPLC–UV assays of im-

munosuppressants are specific and are generally considered the gold standard in the quantification of immunosuppressants. However, they suffer from poor precision, are vulnerable to interferences from matrix and co-administered drugs and require tedious and time-consuming extraction procedures [24]. Even when HPLC was combined with mass spectrometry detection, extensive multi-step extraction procedures (see Table 1) resulting in unacceptable variability were required [31–34]. Most LC–MS/MS assays [35–39] also use multi-step external column extraction procedures, and only LC–MS/MS assays for the quantification of single immunosuppressants have been reported. Here, we describe an LC/LC–MS assay, utilizing automated online sample extraction and a mass-selective detector, that

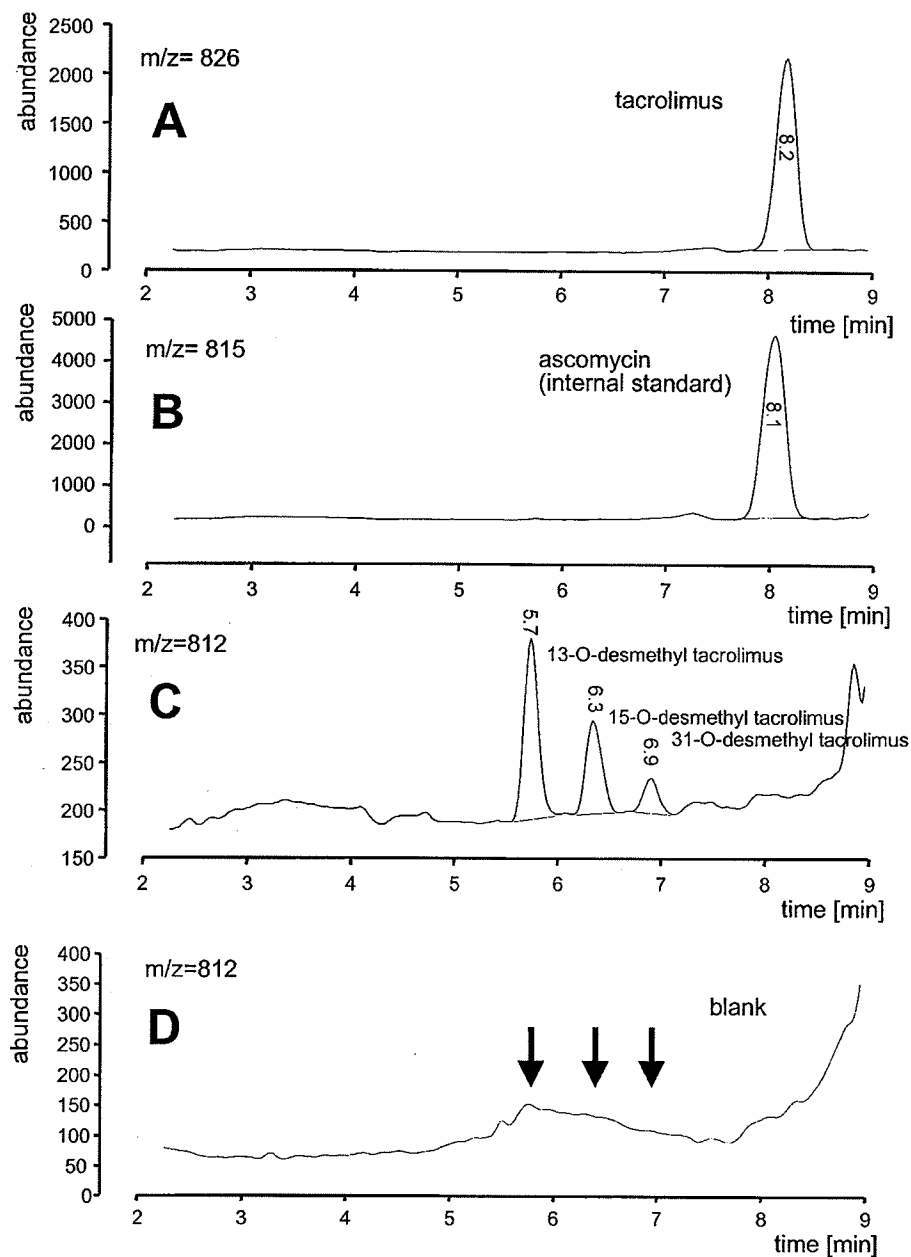


Fig. 4. Representative ion chromatograms of tacrolimus blood samples. Blood samples were taken before and after a healthy volunteer took a single oral 5-mg tacrolimus dose. Ion chromatogram (A) shows tacrolimus ($38.6 \cdot \text{g/l}$, 2.5 h after tacrolimus administration), (B) the internal standard ascomycin ($100 \cdot \text{g/l}$) for the analyses in (A) and (C), (C) the metabolites 13-*O*-desmethyl ($2.2 \cdot \text{g/l}$), 15-*O*-desmethyl ($1.4 \cdot \text{g/l}$) and 31-*O*-desmethyl tacrolimus ($0.73 \cdot \text{g/l}$, same sample as (A) and (B)), and (D) the ion chromatogram ($m/z = 812$, desmethyl tacrolimus) of a blank sample of the same pharmacokinetic profile drawn before tacrolimus administration. The arrows mark the retention times of the tacrolimus metabolite peaks.

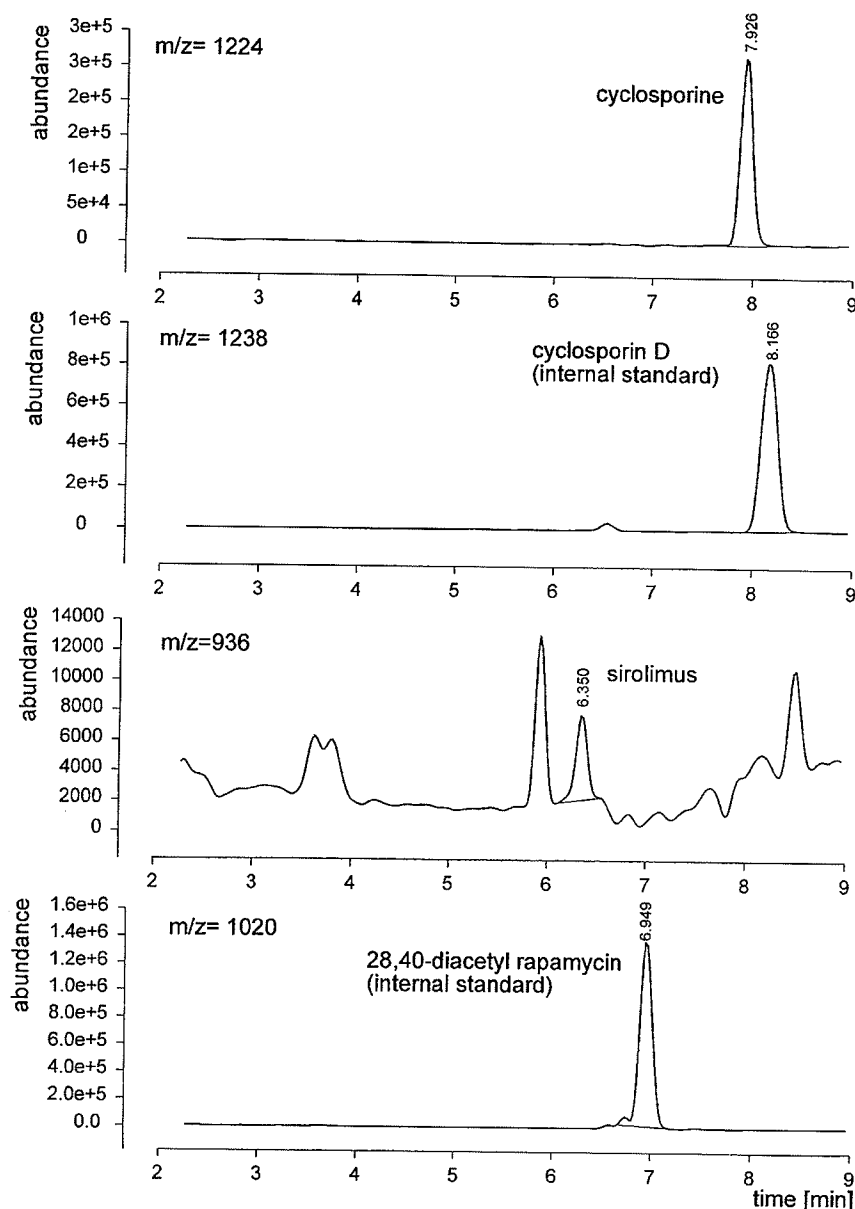


Fig. 5. Representative ion chromatograms of a blood sample from a kidney graft patient 12 h after oral administration of cyclosporine and 8 h after oral administration of sirolimus. Five hundred • g/l cyclosporin D and 100 • g/l 28,40-*O*-diacetyl rapamycin were added as internal standards for cyclosporine and sirolimus, respectively. The concentration of cyclosporine was 162 • g/l and that of sirolimus was 0.55 • g/l.

is integrated into the analytical system as an HPLC component.

Although LC–MS assays have been reported for cyclosporine, tacrolimus, sirolimus and SDZ-RAD,

development of an assay to quantify all four drugs in one assay involved identification of conditions during extraction and HPLC analysis that accommodated the quantification of all study drugs. Potential

problems involved the 10-fold higher therapeutic concentration range of cyclosporine in comparison to that of the macrolide immunosuppressants and the chromatographic conditions necessary to avoid broadening of cyclosporine peaks. As shown, the extraction and LC–MS procedure described above resulted in a lower limit of quantitation that was 5-fold lower than the lower limit of the clinical target concentrations for each of the immunosuppressants, while the linear range of the assay included the concentration ranges relevant for patients.

Although good precision and accuracy of the measurement of immunosuppressant in blood in combination with automated online-extraction can be achieved without addition of internal standards [27–29], we used internal standards for the reasons discussed in detail elsewhere [31–33]. In comparison to other internal standards used for LC–MS quantification of tacrolimus [33,34], ascomycin has the advantage that it is generally available from a commercial source. As an alternative to 28,40-*O*-diacetyl rapamycin, we used 32-desmethoxy rapamycin (Wyeth-Ayerst Research, Pearl River, NY, USA) or 40-*O*-(3-hydroxypropyl) rapamycin (Novartis Pharma, Basel, Switzerland) with similar results. Sirolimus cannot be used as an internal standard for quantification of SDZ-RAD since blood of SDZ-RAD treated patients may contain traces of sirolimus, as a minor SDZ-RAD metabolite [18].

Our assay uses only 100 μ l of blood and therefore allows for quantification of immunosuppressants in small animal studies and pediatric patients [37]. In addition, we avoided the large injection volumes necessary in previously described LC/LC–MS assays [27–29]. The extensive sample preparation procedures used in previously described LC–MS assays for immunosuppressive drugs were necessary since the immunosuppressants distribute mainly into the corpuscular blood components, and whole blood is the recommended matrix for therapeutic drug monitoring [21,22,25]. As for our assay, most other LC–MS assays include a protein precipitation step with ZnSO_4 [27–29,31–34,38]. The automated column extraction procedure was necessary to remove residual blood components and high concentrations of inorganic salt to reduce contamination of the MS source.

Column-switching techniques for automated on-line sample preparation are well established in HPLC analysis [40]. In general, these have worked well with plasma samples and drugs with specific UV-absorption maxima. In comparison to plasma, blood sample preparation is much more complex [41] and both cyclosporine and tacrolimus have UV absorption maxima > 200 nm. Although HPLC–UV assays in combination with column-switching on-line sample preparation have been described for cyclosporine [42–44], the extraction procedures were complicated and time-consuming and those assays have never widely been used. In comparison to HPLC–UV, LC–MS due to its selectivity is more robust against interferences. In our assay, the supernatants after protein precipitation were loaded onto the extraction columns and washed at a high solvent flow of 5 ml/min for 0.7 min. This was a significant improvement over previously published LC–MS assays for immunosuppressants using online sample preparation [27–29] that required an extraction wash step of several minutes. In our experience, column switching sample preparation has not been a significant source of analytical failures.

One of the problems with the HPLC analysis of cyclosporine is peak broadening due to incomplete separation of conformers [45]. Peak broadening is reduced by column temperatures of 65°C and above, and mobile phase pH > 5 [41,45]. An additional reason for the low pH of the mobile phase was the stability of sirolimus, SDZ-RAD and 28,40-*O*-diacetyl rapamycin [32,46].

We took advantage of the automatic bypass valve in the mass selective detector. The mass-selective detector was activated 2 min after the column switch (Fig. 2). Before the bypass valve was activated, material not retained on the column such as inorganic salt was flushed into waste without getting into contact with the electrospray source.

Sodium adduct ions, $[\text{M} + \text{Na}]^+$, gave the strongest signals. Even if 2 mM ammonium acetate was added to the loading buffer and mobile phase to induce formation of $[\text{M} + \text{NH}_4]^+$ at the expense of other ion species, $[\text{M} + \text{Na}]^+$ still gave a significant signal. Addition of sodium ions to the loading buffer and mobile phase, however, almost completely suppressed formation of other ions (Fig. 3). Therefore,

as described previously [27–29,31,32], we decided to focus the mass spectrometer on $[M + Na]^+$ and added sodium formate to the HPLC solvents. Measurement of negative ions was not an option due to the low pH of the mobile phase required.

Our assay separately quantified the major metabolites of the four drugs. Due to the unavailability of authentic metabolite standard materials, no attempt was made to validate quantification of the metabolites. Similar detector responses of the corresponding parent compounds, metabolites and internal standards have been described before [31–34], and indicated that the metabolite concentrations can be estimated by extrapolating from the calibration curves of the parent compounds. This approach is supported by previously reported studies [29,31]. If quantification of the metabolites is not required, the methanol–0.1% formic acid gradient (Table 2) can be replaced by an isocratic elution with methanol–0.1% formic acid (9/1, v/v). This modification results in a 2-min shorter analysis time and a higher sample turn-over.

Our LC/LC–MS assay can easily be adapted to analyze novel immunosuppressants with structures related to cyclosporine, tacrolimus or sirolimus by addition of the corresponding masses to the list of selected ions. In our laboratory, the LC/LC–MS assay served as a platform for the development of assays for other groups of drugs such as HIV protease inhibitors, HMG-CoA reductase inhibitors, azole antifungals, mycophenolic acid and metabolites, as well as losartan and its active major metabolite EXP3174. In most cases, the adaptation involved modification of the loading buffer and focussing the mass spectrometer on the corresponding selected ions. The set up of the LC/LC–MS system as described above, allows us to analyze different drug classes in one automated sequence.

Acknowledgements

The study was supported by the Deutsche Forschungsgemeinschaft grants Ch95/6-2 (U.C.), Se985/1-1 (N.S.), and SFB265 A7 (G.I.K., K.F.S.) as well as NIH grants CA72006 and GM26691 (L.Z.B.).

References

- [1] B.D. Kahan, *New Engl. J. Med.* 321 (1989) 1725.
- [2] D. Faulds, K.L. Goa, P. Benfield, *Drugs* 45 (1993) 953.
- [3] D.H. Peters, A. Fitton, G.L. Plosker, D. Faulds, *Drugs* 46 (1993) 746.
- [4] S.L. Schreiber, *Science* 251 (1991) 283.
- [5] W. Schuler, R. Sedrani, S. Cottens, B. Haberman, M. Schulz, H.-J. Schuurman, G. Zenke, H.G. Zerwes, M.H. Schreier, *Transplantation* 64 (1997) 36.
- [6] T. Boehler, J. Waiser, K. Budde, S. Lichter, A. Jauho, L. Fritsche, A. Korn, H.H. Neumayer, *Transplant. Proc.* 30 (1998) 2195.
- [7] H.-J. Schuurman, S. Cottens, S. Fuchs, J. Joergensen, T. Meerloo, R. Sedrani, M. Tanner, G. Zenke, W. Schuler, *Transplantation* 64 (1997) 32.
- [8] S.M. Stepkowski, L. Tian, K.L. Napoli, R. Ghobrial, M.E. Wang, T.C. Chou, B.D. Kahan, *Clin. Exp. Immunol.* 108 (1997) 63.
- [9] S.M. Stepkowski, K.L. Napoli, M.E. Wang, X. Qu, T.C. Chou, B.D. Kahan, *Transplantation* 62 (1996) 986.
- [10] B.D. Kahan, B.A. Julian, M.D. Pescovitz, Y. Vanrenterghem, J. Neylan, *Transplantation* 68 (1999) 1526.
- [11] B. Hausen B, T. Ikonen, N. Briffa, G.J. Berry, U. Christians, R.C. Robbins, L. Hook, N. Serkova, L.Z. Benet, W. Schuler, R.E. Morris, *Transplantation* 69 (2000) 76.
- [12] D.M. Vu, S. Qi, D. Xu, J. Wu, W.E. Fitzsimmons, S.N. Sehgal, L. Dumont, S. Busque, P. Daloze, H. Chen, *Transplantation* 64 (1997) 1853.
- [13] V.C. McAlister, Z.H. Gao, K. Peltekian, J. Domingues, K. Mahalati, M.S. MacDonald, *Lancet* 355 (2000) 376.
- [14] J.L. Miller, *Am. J. Health Syst. Pharm.* 56 (1999) 2177.
- [15] R. Sedrani, S. Cottens, J. Kallen, W. Schuler, *Transplant. Proc.* 30 (1998) 2192.
- [16] T. Kronbach, V. Fischer, U.A. Meyer, *Clin. Pharmacol. Ther.* 43 (1998) 630.
- [17] M. Sattler, F.P. Guengerich, C.H. Yun, U. Christians, K.F. Sewing, *Drug Metab. Dispos.* 20 (1992) 753.
- [18] W. Jacobsen, N. Serkova, K. Hallensleben, K. Sewing, L.Z. Benet, U. Christians, *ISSX Proc.* 15 (1999) 117.
- [19] A. Lo, G.J. Burckhart, *J. Clin. Pharmacol.* 39 (1999) 995.
- [20] J.F. Trotter, *Semin. Gastroenterol. Dis.* 9 (1998) 147.
- [21] M. Oellerich, V.W. Armstrong, B.D. Kahan, L. Shaw, D.W. Holt, R.W. Yatscoff, A. Lindholm, P. Halloran, K. Gallicano, K. Wonigeit, E. Schuetz, H. Shran, T. Annesley, *Ther. Drug Monit.* 17 (1995) 643.
- [22] W.J. Jusko, A.W. Thomson, J.J. Fung, P. McMaster, P.H. Wong, E. Zylber-Katz, U. Christians, W. Fitzsimmons, R. Lieberman, J. McBride, M. Kobayashi, S.J. Soldin, *Ther. Drug Monit.* 17 (1995) 606.
- [23] L.M. Shaw, D.W. Holt, P. Keown, R. Venkataraman, R.W. Yatscoff, *Clin. Ther.* 21 (1999) 1632.
- [24] A. Johnston, D.W. Holt, *Br. J. Clin. Pharmacol.* 47 (1999) 339.
- [25] R.W. Yatscoff, R. Boeckx, D.W. Holt, B.D. Kahan, D.F.

- LeGatt, S. Sehgal, S.J. Soldin, K. Napoli, C. Stiller, *Ther. Drug Monit.* 17 (1995) 676.
- [26] K.L. Napoli, B.D. Kahan, *Transplant. Proc.* 30 (1998) 2189.
- [27] C. Vidal, G.I. Kirchner, G. Wuensch, K.F. Sewing, *Clin. Chem.* 44 (1998) 1275.
- [28] G.I. Kirchner, C. Vidal, W. Jacobsen, A. Franzke, K. Hallensleben, U. Christians, K.F. Sewing, *J. Chromatogr. B* 721 (1999) 285.
- [29] G.I. Kirchner, C. Vidal, M. Winkler, L. Mueller, W. Jacobsen, A. Franzke, K.F. Sewing, *Ther. Drug Monit.* 21 (1999) 116.
- [30] IUPAC Nomenclature of Organic Chemistry. A Guide to IUPAC Nomenclature of Organic Components (recommendations 1993). Blackwell Scientific Publications, Boston, MA, 1993.
- [31] F. Streit, U. Christians, H.M. Schiebel, K.L. Napoli, L. Ernst, A. Linck, B.D. Kahan, K.F. Sewing, *Clin. Chem.* 42 (1996) 1417.
- [32] I. Segarra, T.R. Brazelton, N. Gutermann, B. Hausen, R.E. Morris, L.Z. Benet, U. Christians, *J. Chromatogr. B* 720 (1998) 179.
- [33] U. Christians, F. Braun, M. Schmidt, N. Kosian, H.M. Schiebel, L. Ernst, M. Winkler, C. Kruse, A. Linck, K.F. Sewing, *Clin. Chem.* 38 (1992) 2025.
- [34] A.K. Gonschior, U. Christians, M. Winkler, H.M. Schiebel, A. Linck, K.F. Sewing, *Ther. Drug Monit.* 17 (1995) 504.
- [35] P.J. Taylor, A. Jones, G.A. Balderson, S.V. Lynch, R.L. Norri, S.M. Pond, *Clin. Chem.* 42 (1996) 279.
- [36] A.M. Alak, S. Moy, M. Cook, P. Lizak, A. Niggebiugge, S. Menard, A. Chilton, *J. Pharm. Biomed. Anal.* 16 (1997) 7.
- [37] P.J. Taylor, C.E. Jones, P.T. Martin, S.V. Lynch, A.G. Johnson, S.M. Pond, *J. Chromatogr. B* 705 (1998) 289.
- [38] P.J. Taylor, A.G. Johnson, *J. Chromatogr. B* 718 (1998) 251.
- [39] Q. Zhang, J. Simpson, H.I. Aboleneen, *Ther. Drug Monit.* 19 (1997) 470.
- [40] R. Huber, K. Zech, in: R.W. Frei, K. Zech (Eds.), *Selective Sample Handling and Detection in High-Performance Liquid Chromatography*, *J. Chromatogr. Library*, Vol. 39A, Elsevier, Amsterdam, 1988, pp. 81–144.
- [41] U. Christians, K.F. Sewing, in: K. Zech, R.W. Frei (Eds.), *Selective Sample Handling and Detection in High-Performance Liquid Chromatography*, *J. Chromatogr. Library*, Vol. 39B, Elsevier, Amsterdam, 1989, pp. 82–132.
- [42] D.J. Gmur, P. Meier, G.C. Yee, *J. Chromatogr.* 425 (1988) 343.
- [43] H.T. Smith, W.T. Robinson, *J. Chromatogr.* 305 (1984) 353.
- [44] P.E. Wallemacq, M. Lesne, *J. Chromatogr.* 413 (1987) 131.
- [45] L.D. Bowers, S.E. Mathews, *J. Chromatogr.* 333 (1985) 231.
- [46] P.C. Wang, K.W. Chan, R.A. Schiksnis, J. Scatina, S.F. Sisenwine, *J. Liq. Chromatogr.* 17 (1994) 3383.